A Nuclear Interferometer for Ultra-Light Dark Matter Detection

Hannah Banks,[1, 2] Elina Fuchs,[1, 3, 4] and Matthew McCullough[1]

[1]*CERN, Theoretical Physics Department, Geneva, Switzerland*

[2]*DAMTP, University of Cambridge, Wilberforce Road, Cambridge, UK*

[3]*Institute of Theoretical Physics, Leibniz Universität Hannover, Appelstr. 2, 30167 Hannover, Germany*

[4]*Physikalisch-Technische Bundesanstalt (PTB), Bundesallee 100, 38116 Braunschweig, Germany*

Abstract

We propose the nuclear interferometer - a single-photon interferometry experiment based upon the thorium-229 nuclear clock transition - as a novel detector for ultra-light dark matter (ULDM). Thanks to the enhanced sensitivity of this transition to the variation of fundamental constants, we find that possible realisations of such an experiment deploying either single ions or clouds of atoms have the potential to complement advanced very-long-baseline terrestrial clock atom interferometers in the search for ultra-light dark matter with scalar couplings to photons in the future. Nuclear interferometry may also offer an unparalleled window to new physics coupling to the QCD sector via quarks or gluons, with a discovery reach that could enhance existing and proposed experiments over a range of frequencies in the direction of well-motivated parameter space.

I. INTRODUCTION

The hunt for dark matter (DM) is entering a new era. Despite a panoply of evidence for its existence, very little is known about the nature or properties of DM on the particle level. At present, our only real handle on this elusive substance comes from observations of its gravitational interactions over astrophysical and cosmological scales, leaving its microphysics largely unconstrained. Even under the assumption that the energy density attributed to DM is predominantly harboured by a single species, the mass in question could viably range from $\sim 10^{-22}$ eV bosons up to $\sim 10^{19}$ GeV mass primordial black holes [1, 2]. Deciphering the fundamental constituents of DM and its particle-like properties remains of upmost priority in contemporary particle physics.

Over the last few decades, non-gravitational interactions of weak-scale particles have been relentlessly pursued as part of a broad experimental campaign encompassing direct, indirect and collider based searches, all to no avail [3]. Whilst there remain a number of interesting and well-motivated avenues in the vicinity of this parameter space yet to explore, the idea that DM instead comprises sub-eV ultra-light bosonic particles which have remained hidden thus far due to extremely feeble couplings to the Standard Model (SM), has gained significant traction in recent years [4, 5]. A number of highly motivated DM candidates fall into this category including the QCD axion [6, 7] (see Ref. [8] for a review) and other pseudo-scalar axion-like particles (ALPs), vector dark photons [9–11] and scalars such as moduli [12–15], dilatons [16, 17], Higgs portal dark matter [18] and the relaxion [19, 20].

The high occupation numbers required for such a light species to saturate the relic local dark matter density renders its behaviour over galactic scales akin to that of a coherent, classical wave, giving rise to a host of novel phenomenological signatures which are not shared by heavier 'particle-like' candidates [21, 22]. Direct searches for ultra-light DM (ULDM) thus typically rely upon different detection strategies to the traditional experiments conceived for weak-scale candidates which seek impulses resulting from particle-like interactions. Recent advances in quantum sensing technologies have been transformative in this respect, opening up a number of exciting new possibilities to probe new light weakly coupled states which lie within this 'precision' frontier [23–27].

ULDM could conceivably couple to the SM through a number of different 'portals', each of which has a distinct set of phenomenological consequences and in turn, experimental signatures. In this proposal we focus specifically on *scalar* ULDM with linear couplings to the SM. These couplings cause fundamental constants, and thus physical properties such as atomic energy levels and the distance scales which they govern, to oscillate in time at a frequency set by the DM mass, see e.g. Refs. [24, 28–31]. This effect can be searched for in a variety of different ways including accelerometers [32], optical cavities [33], mechanical resonators [34, 35] and by comparing the frequency of two different atomic (see e.g. Refs. [29, 31, 36, 37]) or molecular [38] clocks. More recently, atom interferometers have been identified to offer the potential to probe ULDM-induced oscillations of atomic transition frequencies in a complementary region of parameter space to the aforementioned tests [39, 40]. In its most basic form, an atom interferometer constitutes an experiment which measures the phase differ-

ence between two spatially delocalised quantum superpositions of clouds of atoms [41]. Such experiments can be thought of analogously to optical interferometers but with the traditional beam-splitters and mirror elements realised via a sequence of controlled duration laser pulses which act to divide, reflect and recombine the atomic wave-packets by driving transitions between internal energy states. The presence of ULDM can be diagnosed by the existence of an oscillating phase difference between a pair of spatially separated single-photon[1] atom interferometers which are resonantly interrogated with common laser pulses [40]. Such multi-atom interferometer configurations are termed single-photon atom gradiometers and have the key advantage in that noise arising from fluctuations and jitters in the laser phase is common to both instruments and thus cancels in the differential measurement [43]. In order to achieve sensitivity to ULDM, such proposals look to both long ($\mathcal{O}(km)$) baselines and large-momentum-transfer (LMT) atom optics[2] [47] (see Sec. II B) to increase the recorded phase difference. To sustain these practices it is essential for the pair of internal states on which the atom interferometer is based to be sufficiently long-lived such that spontaneous emission, which would otherwise exponentially degrade the sensitivity due to loss of coherence, is not significant.[3] For the very long baselines and high number of sequential pulses demanded by ULDM searches (see e.g. [50, 51]), ultra-narrow transitions such as those deployed in optical lattice clocks are therefore typically taken advantage of. For this reason such atom interferometer realisations have earned the title of 'large-momentum-transfer clock atom interferometry' [52].

A number of prototype long-baseline gradiometers including AION-10 [53], MAGIS-100 [54] and VLBAI [55] are currently in development, and will serve as essential technological readiness indicators to longer (up to km-scale) instruments envisioned to offer sensitivity to oscillating ULDM as well as mid-frequency (0.1-10 Hz) gravitational waves by the mid 2030's. A comprehensive overview of the potential capabilities of long-baseline interferometers in addition to their current status of development can be found in Ref. [52].

In tandem, the discovery of an excited isomeric state

in ^{229}Th [56, 57], has led to proposals for a 'nuclear clock' [58–60] based on transitions between the ground and the ^{229m}Th excited isomer state. Arising due to accidental cancellations between contributions from strong and electromagnetic interactions [61–63], the small (8.3 eV [64]) gap in energy between the ground and excited states lies in the optical range [65] and offers an enhanced sensitivity to the variation of fundamental constants at the level of several orders of magnitude [61, 66–68] over typical optical clock transitions in atoms, ions and highly charged ions [69]. Frequency comparisons between nuclear and atomic optical clocks could offer a highly sensitive probe of ULDM in the near future [29, 70–73], and the (still broad) lineshape already constrains the ULDM parameter space [74]. Due to rapid internal conversion, the excited isomeric state in electrically neutral ^{229}Th is short-lived with a half-life of $\sim 7\,\mu s$ [75]. Proposed realisations of the thorium nuclear clock for deployment in such experiments therefore look to either ionic forms [59] or to a thorium-doped lattice [76] in which internal conversion is forbidden and the isomeric state becomes long-lived with a radiative lifetime of $\sim 10^4$ s [70].

Whilst the nuclear clock is yet to be realised experimentally, rapid progress towards this goal has been made in recent years and especially months. The production of ^{229}Th at ISOLDE at CERN via the decay chain of ^{229}Fr as a new pathway [77] refined the knowledge of the nuclear transition energy from the percent to the permill level. Subsequently, based on the development of a new tunable VUV laser [78], the first laser excitation of the ^{229}Th nucleus was achieved at PTB [79] in Th-doped crystals [80]. While the resolution of the transition frequency here is limited by the laser linewidth to 7 GHz [79], corresponding to a relative uncertainty of $\mathcal{O}(10^{-6})$, this precision has since further been improved to 3 GHz at UCLA [81] and, by means of a VUV frequency comb at JILA, to 300 kHz [82], suppressing the relative uncertainty to $\mathcal{O}(10^{-10})$. With such developments rapidly paving the way towards an operational nuclear clock, the time to investigate other ways in which this unique transition could be exploited to probe fundamental physics is ripe.

In this work we propose to amalgamate the ^{229}Th nuclear clock transition with the established principles of single-photon matter-wave interferometry to form what we shall refer to as a 'nuclear interferometer'. We present two different possible realisations of this idea - one based on single ^{229}Th ions and the other on clouds of neutral ^{229}Th atoms. Whilst both present additional experimental challenges beyond those of the optical clock transitions of conventional atom interferometry-based ULDM search proposals, we find that for certain experimental configurations, the enhanced sensitivity of the ground-to-excited state transition to the variation of fundamental constants in these thorium systems is able to overcome the loss in sensitivity that respectively results from the

---

[1] Here, 'single-photon' refers specifically to a class of interferometers in which the desired transition is driven by a single laser frequency. This contrasts with interferometers based on Raman transitions which involve two distinct optical fields (see e.g. Ref. [42]).

[2] Such techniques (see e.g. Refs. [44–46]) effect an increase of the physical baseline by employing an increased number of laser pulses to augment the momentum transfer between the two arms of each atom interferometer and in turn the phase difference accumulated at the end of the sequence.

[3] For a discussion of some of the potential implications of spontaneous decay on long-baseline atom interferometry in space, see Refs. [48, 49].

low ion flux (i.e large quantum projection noise) and the short lifetime of the excited state in neutral form, to offer access to new regions of ULDM parameter space.

We begin in Sec. II A by introducing the ULDM model that we will adopt as an example in this work, before computing the signal that it would imprint in a generic nuclear interferometry experiment in Sec. II B. In Sec. II C we then derive an expression for the reach of a general free-fall nuclear interferometer assuming shot-noise limited detection, in terms of a handful of tunable parameters which characterise the experimental operating configurations. In Sec. III we explore two different ways, making use of single-ion clocks and clouds of atoms respectively, in which such a nuclear interferometer could be realised experimentally and discuss how the aforementioned principles apply to each case. The challenges of working with both systems are discussed and any requisite technological advancements outlined. Forecasts of the sensitivity of both realisations to scalar ULDM with linear couplings to SM operators for a variety of experimental configurations that may become feasible in the future are presented in Sec. IV and compared to bounds from existing experiments and the predicted sensitivities of competing proposals. Some concluding remarks are offered in Sec. V.

II.   THE CONCEPT

A.   Ultra-light scalar Dark Matter

To motivate this proposal we consider an ultra-light singlet scalar field, ϕ, which couples linearly[4] to the SM by way of non-derivative operators. We assume that this field comprises an $\mathcal{O}(1)$ fraction[5] of the local DM abundance. Working in units in which $\hbar = c = 1$ and following the notational conventions[6] of Refs. [29, 85] in parameterising the dimensionless couplings relative to Newton's gravitational constant G_N, the leading-order low energy Lagrangian, applicable to scales $\gtrsim 1$ GeV, can be expressed in terms of a relatively minimal set of operators

---

[4] Note that quadratic couplings also lead to the variation of fundamental constants [83], and become relevant if linear couplings are not present, forbidden for instance by a symmetry. We leave consideration of such couplings to future work.

[5] An exploration of the ability of scalar couplings to generate the correct relic abundance can be found in Ref. [84].

[6] In this paramaterisation, the coefficients and normalisation of each of the terms in the Lagrangian are specifically chosen such that the dimensionless couplings are all RG-invariant [85].

as

$$\mathcal{L}_\phi = -\kappa\phi\left[\frac{d_e}{4e^2}F_{\mu\nu}F^{\mu\nu} - \frac{d_g\beta_3}{2g_3}G^A_{\mu\nu}G^{A\mu\nu} - d_{m_e}m_e\bar{e}e \right.$$
$$\left. - \sum_{i=u,d}(d_{m_i} + \gamma_{m_i}d_g)\, m_i\bar{\psi}_i\psi_i\right],$$

(1)

where $F_{\mu\nu}$, $G_{\mu\nu}$ are respectively the photon and gluon field strength tensors and e, ψ_i are the fermion fields of the first generation. Here, $\kappa = \sqrt{4\pi G_N}$, $\beta_3(g_3)$ is the QCD beta function, g_3 is the strong coupling constant and the γ_{m_i}, $i = \{u, d\}$ are the anomalous dimensions of the u and d quarks.

These effective operators feature in several well-motivated models of ultra-light dark matter. For one example, in the presence of additional sources of CP violation beyond those included within the SM, both the QCD axion, and other pseudo-scalar axion-like particles possess CP-even scalar couplings in addition to their CP-odd pseudo-scalar interactions. In particular, the QCD axion can attain a non-zero scalar coupling to quarks [86–88], which is bounded from below by the CP violation in the SM, and from above by measurements of the neutron electric dipole moment.

Owing to the high occupation numbers and small velocities of DM in the Milky Way, ϕ can be well approximated by a non-relativistic temporally and spatially oscillating classical plane wave

$$\phi(t, \mathbf{x}) = \phi_0 \cos[m_\phi(t - \mathbf{v}\cdot\mathbf{x}) + \theta] + \mathcal{O}(|\mathbf{v}|^2)\,, \quad (2)$$

with an amplitude $\phi_0 \simeq \sqrt{2\rho_{\mathrm{DM}}}/m_\phi$ which is set by the requirement that the field saturates the local DM energy density, $\rho_{\mathrm{DM}} = 0.3$ GeV cm^{-3} [89]. θ denotes an arbitrary phase. The field is temporally coherent over a coherence time $\tau_c = 2\pi/(m_\phi\sigma_v^2)$ and spatially coherent over a coherence length $\lambda_c = 2\pi/(m_\phi\sigma_v)$ [90] where $\sigma_v \sim \sqrt{\langle(\mathbf{v} - \langle\mathbf{v}\rangle)^2\rangle} \sim 5\times 10^{-4}$ (in natural units) [91] is the DM virial velocity.

B.   The signal

The couplings in Eq. 1 cause the fine structure constant α, the strong coupling constant α_s and the fermion masses to vary in time. Explicitly,

$$m_\psi = m_\psi\left[1 + d_{m_\psi}\kappa\phi(t, \mathbf{x})\right] \quad (3)$$
$$\alpha = \alpha\left[1 + d_e\kappa\phi(t, \mathbf{x})\right] \quad (4)$$
$$\alpha_s = \alpha_s\left[1 + d_g\kappa\phi(t, \mathbf{x})\right] \quad (5)$$

where ψ represents a generic fermion with mass m_ψ.

These variations induce oscillations in the nuclear energy and length scales and, in turn, the thorium nuclear transition energy, $\omega_N = 8.3\,\mathrm{eV}$ [64]. ω_N is a function, g, of both α and the ratio $X_q = m_q/\Lambda_{\mathrm{QCD}}$, i.e.

$$\omega_N = g(\alpha, X_q) \ . \tag{6}$$

Here, the QCD scale Λ_{QCD}, is defined to be the Landau pole of the running of the strong coupling constant as a function of an energy scale μ, $\alpha_s(\mu) \sim 1/\ln(\Lambda_{\mathrm{QCD}}/\mu)$, and is thus related to α_s via dimensional transmutation.

As such, in the presence of the scalar DM background ω_N oscillates as

$$\omega_N = \omega_N + \Delta\omega_N \ , \tag{7}$$

where [66, 67]

$$\Delta\omega_N = \omega_N \left(\frac{\partial \ln g}{\partial \ln \alpha} \frac{\Delta\alpha}{\alpha} + \frac{\partial \ln g}{\partial \ln X_q} \frac{\Delta X_q}{X_q} \right) \tag{8}$$

$$\approx \omega_N \left(10^4 d_e + 10^5 (d_{\hat{m}} - d_g) \right) \phi(t, \mathbf{x}) \ . \tag{9}$$

In this expression $d_{\hat{m}}$ is defined to be the coupling to the symmetric combination of quark masses:

$$d_{\hat{m}} \equiv \frac{d_{m_d} m_d + d_{m_u} m_u}{m_d + m_u} \ . \tag{10}$$

We now investigate how these oscillations would manifest in a future nuclear interferometer experiment. Fig. 1 shows a space-time diagram of the interferometer sequence proposed for a vertical single-photon atom gradiometer composed of a pair of interferometers situated at positions z_1 and z_2 respectively. This scheme deploys large-momentum-transfer (LMT) techniques [47] in order to increase the momentum transfer between the two arms of each interferometer and in turn the sensitivity. In practice this involves realising the beam-splitter with $n > 1$ laser pulses which each impart a momentum $\hbar\mathbf{k}$ where $\mathbf{k}$ denotes the photon wavevector, to one of the interferometer arms.

The phase difference between the two arms of each isolated interferometer at the end of the interferometer sequence receives contributions from multiple sources. In the absence of new physics, the phase accumulated on each of the two arms is expected to cancel due to the symmetry of the interferometric sequence. It suffices therefore to only track the ULDM-induced phase accumulated by the excited state relative to the ground state over each arm of the interferometer.

For a segment of the trajectory between times t_0 and t_1 during which the system is in the nuclear excited state, the ULDM-induced phase that is accrued (relative to the
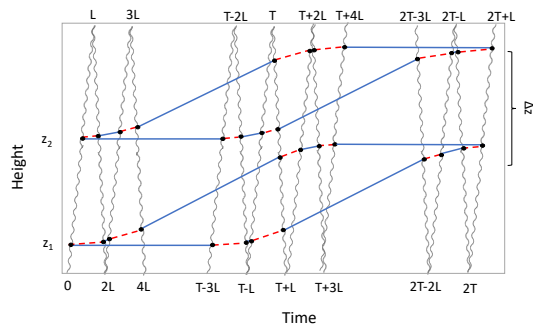

FIG. 1. A schematic spacetime diagram of a vertical single-photon atom gradiometer with $n = 4$ large-momentum-transfer atom optics. The experiment comprises a pair of single-photon atom interferometers based on single-photon transitions between a ground (blue) and excited (red) state. The wavy lines denote laser pulses fired from opposite ends of the baseline which are used to divide, direct and recombine the atomic states to yield an interference pattern. Atom-laser interactions are shown as black circles.

ground state) is

$$\Phi_{t_0}^{t_1} \equiv \overline{\Delta\omega_N} \int_{t_0}^{t_1} \mathrm{d}t \ \cos(m_\phi t + \theta) \ , \tag{11}$$

where we have defined

$$\overline{\Delta\omega_N} = \omega_N \kappa \phi_0 (10^4 d_e + 10^5 (d_{\hat{m}} - d_g)) \ , \tag{12}$$

to be the magnitude of $\Delta\omega_N$.

The total phase difference recorded by a single interferometer follows from subtracting the total phase (relative to the ground state) that is accumulated on each of the two arms during propagation in the excited state.

The gradiometer signal, Φ_s, then corresponds to the difference between the phase difference recorded by the interferometer located at position z_1 and that recorded by the interferometer at position z_2. For the interferometric sequence depicted in Fig. 1, in the limit that the launch velocity in the two interferometers is the same, the gradiometer signal can be shown (see Ref. [92] for a derivation) to be

$$\Phi_s \approx \frac{\Delta z}{L} \left(\left[\Phi_{T-(n-1)L}^{T+L} - \Phi_0^{nL} \right] - \left[\Phi_{2T-(n-1)L}^{2T+L} - \Phi_T^{T+nL} \right] \right) \ , \tag{13}$$

where the interrogation time T is half the time between the two beam-splitter sequences, and $\Delta z = |z_1 - z_2|$ is the vertical separation of the two interferometers.[7] n refers to the number of large-momentum-transfer (LMT) kicks

—————

[7] For very long-baseline gradiometers such as those considered in

applied, i.e. the total number of pulses used to realise each beam-splitter sequence.

The signal amplitude $\overline{\Phi}_s$ for a single phase measurement, defined according to

$$\overline{\Phi}_s \equiv \left(\frac{1}{\pi} \int_0^{2\pi} \mathrm{d}\theta \ \Phi_s^2 \right)^{1/2} , \tag{14}$$

can then be shown to be [92]

$$\overline{\Phi}_s = 8 \frac{\overline{\Delta\omega_N}}{m_\phi} \frac{\Delta z}{L} \sin\left[\frac{m_\phi(T - (n-1)L)}{2} \right] \\ \times \sin\left[\frac{m_\phi nL}{2} \right] \sin\left[\frac{m_\phi T}{2} \right] . \tag{15}$$

In order to isolate the dependence of this signal on the scalar couplings we introduce the notation

$$\overline{\Phi}_s = d_\phi \overline{\Phi}_R , \tag{16}$$

where

$$d_\phi = d_e + 10(d_{\hat{m}} - d_g) . \tag{17}$$

C. Experimental Sensitivity

We now quantify the reach of a potential nuclear interferometer as an ULDM detector. In practice, over an experimental campaign of duration T_{int}, a total of N measurements of the gradiometer phase difference will be performed at a regular sampling interval $\Delta t = T_{\text{int}}/N$, corresponding to a constant shot repetition rate. Such measurements will contain, in addition to any possible ULDM-induced signal, contributions from background noise sources.

Assuming that the sensitivity is limited by the quantum projection noise (or shot-noise) of the interrogated species with spectral density S_{n}, the minimum scalar coupling d_ϕ^* that could be detected at a signal-to-noise ratio SNR following a measurement period T_{int} is

$$d_\phi^* \simeq \frac{\sqrt{\text{SNR}}}{\overline{\Phi}_R} \times \sqrt{\frac{S_{\text{n}}}{T_{\text{int}}} \times \max\left(1, \sqrt{\frac{T_{\text{int}}}{\tau_c}}\right)} . \tag{18}$$

Further details regarding the origin of this expression are

———

Ref. [40], the approximation $\Delta z/L \sim 1$ is often adopted. In more compact gradiometers including some of those considered in this work, this factor can be an important correction and needs to be explicitly considered.

given in Appendix A.

Inserting Eq. 15 and Eq. 16 into Eq. 18, one finds that the experimental sensitivity depends on the parameters T, L, n which are set in the experimental design, in addition to the shot-noise spectral density S_{n} and the campaign duration T_{int}. For a gradiometer comprising two identical interferometers, the shot-noise can be described by the white noise spectrum [92–94]

$$S_{\text{n}} = \frac{2\Delta t}{C^2 N_{\text{s}}} , \tag{19}$$

where N_{s} is the number of atoms (ions) per shot and the interferometer contrast, $C \leq 1$, characterises the amplitude of the oscillations of the probability of being in the ground and excited states.

The values that these parameters can take depend both on the physical nature of the source (i.e. whether one is working with atoms or ions) and on the properties of the transition, including, most importantly for the scenarios to be considered in this work, its width. In clock interferometry, for which spontaneous decay of the excited state can be neglected, S_{n} is independent of the choice of T, n and L for a given set of starting conditions (i.e. the number of species per shot). Given the increase in the signal phase difference with n, L and T, such experiments look to maximise these parameters. Due to the geometric requirement that the interrogated clouds remain within the baseline for the duration of the interferometric sequence, it is important to realise that these parameters cannot be extremised independently. Any given choice of L restricts the maximum LMT order n and interrogation time T that can be implemented without the trajectories of the interrogated species exceeding the baseline.

The picture is more nuanced if one considers operating on a broad transition for which spontaneous decay becomes important relative to the proposed interferometer scales. Here, the increase in the phase shift that comes with increasing L and n is accompanied by a degradation of the interferometer contrast and the number of species in the cloud at the point of detection relative to their input design values due to the enhanced degree of spontaneous decay. Precisely which of these two parameters is degraded depends on where in the interferometric cycle the decay occurs and how far the decayed species have travelled away from the cloud before the end of the sequence. Those that have left the cloud contribute to a reduction in N_{s} whereas those which have lost coherence with the cloud due to decay but have not had time to travel significantly, form a diffuse background reducing C [95]. Both of these effects manifest as an exponential increase in the shot-noise spectrum with the product nL which, as we shall see, ultimately limits both the baseline and the LMT order that can be usefully deployed in such experiments.

Before moving on we comment on the assumption that the experimental sensitivity is shot-noise limited. Achieving shot-noise limited detection is a key design goal for any atomic sensor and requires, by definition, that all other sources of noise arising from both systematic and stochastic effects, are subdominant. Whilst this ideal has already been demonstrated experimentally for small-scale table-top atom interferometers (see e.g. Refs. [96–98]), scaling the experiments up to longer baselines brings additional considerations and challenges for noise control. Comprehensive assessments of the many sources of noise relevant to long-baseline atom interferometry (e.g. gravity gradients, laser phase noise, mechanical vibrations etc.), in addition to the various practices and techniques that may be deployed to control these, have been discussed at length in literature (see e.g. Refs. [54, 99–101]) and used to place requirements on various aspects of the experimental operation. Where not already achievable with current technologies, these stand as targets for ongoing research and development. Given that the arguments for many of these noise sources carry over straightforwardly to both of the nuclear interferometry realisations presented in this work, we do not attempt to replicate this discussion, assuming that such conditions and practices could also be successfully applied to any future nuclear interferometer experiment. Instead, in Sec. III we identify just the most significant sources of noise that are likely to impact each of the proposals outlined in this work, compare them to the shot-noise floor and discuss any resulting implications for the instrument design or experimental operation.

III. POSSIBLE REALISATIONS

We now discuss two distinct ways in which the principles outlined in the previous sections could be applied to perform interferometry on the ground-excited isomeric state transition in ^{229}Th in the future - the first involving single-ion 'clocks', and the second clouds of neutral atoms. Both scenarios present a distinct set of experimental challenges from the sources traditionally considered for long-baseline interferometry, yet, as will be shown, may offer the potential to open up new phenomenological territory in the future provided the requisite technologies can be developed. Differing both in their physical nature and the properties of the ground-excited state transition, these two realisations demand starkly different operating configurations (as characterised by the parameters identified in Sec. II C) which we now outline.

A. Single Ions

As previously discussed, conventional ULDM searches using atom interferometry propose to make use of ultra-narrow clock transitions which, thanks to long excited state lifetimes, allow for the use of long baselines and large inter-arm momentum transfers. Although the excited isomeric state lifetime for *neutral* ^{229}Th is only $\sim 10^{-5}$ s [75] due to internal conversion, when ionised, this decay channel becomes inaccessible and the (now radiative decay limited) lifetime is of order $\sim 10^4$ s [77, 102], falling within the remits of clock interferometry. We thus begin our exploration of the potential usage of ^{229}Th in free-fall matter-wave interferometry by considering working with an ionic[8] form.

Unlike for a neutral species which could (providing sufficient cooling is achieved to prevent significant Doppler expansion of the cloud) potentially be launched in clouds comprising up to $10^8 - 10^{10}$ simultaneously interrogated atoms, with ions electrostatic repulsion prohibits more than a single ion per shot (i.e. $N_s = 1$). Whilst, at least when exploited for fundamental physics, atom interferometers typically seek to maximise the number of atoms per shot in an effort to minimise quantum projection noise, experiments working with single atoms in free-fall have already been both conceived and performed [103].

In addition to deploying a high number of atoms per shot, the sensitivity forecasts for long-baseline atom interferometers also make use of multiplexing (see e.g. Ref. [52]). Exploiting the Doppler shift to the transition frequency experienced by clouds of atoms moving at different velocities, this technique allows the time interval between successive shot launches to be reduced below the interferometer period (2T) with multiple independent interferometers concurrently in operation. Since (in typical Mach-Zehnder interferometry schemes) the atoms are launched upwards and subsequently fall under gravity, the trajectories of atoms in successive clouds cross. The atoms, which can be treated ballistically, are effectively non-interacting such that this trajectory overlap can occur without disrupting the generation of interference at detection. The same can not be said for ions due to electrostatic repulsion. This imposes a lower limit on the time interval between shots: $\Delta t \geq 2T$. We note that whilst this condition applies to interferometry configurations in which the ions are launched upwards and latterly fall under gravity as in this proposal, if instead a configuration could be utilised in which they only travelled in one direction (i.e. if dropped from rest with the primary

---

[8] From the perspective of the interferometry sequence, the precise charge of the ion is unimportant and we thus leave this unspecified.

laser pulses fired vertically downwards) such that they were detected in a different region from launch, it could be possible to achieve a higher effective shot flux due to the possibility of now applying multiplexing. In this case the experimental parameters would need to be carefully selected in order to ensure that there are no intersections between the trajectories of each of the arms of the two interferometers. In order for such linear, non-intersecting trajectories to simultaneously satisfy the geometric constraints of the baseline, smaller T, n and Δz than the conventional set-up are likely to be necessary, somewhat suppressing the potential sensitivity gain associated with a higher ion flux. We leave a more detailed exploration of the potential benefit of such scenarios to future work.

In order to mitigate the inherently large quantum projection noise associated with working with single ions and thus optimise the sensitivity to ULDM of such an experiment, it is favourable to deploy both high LMT orders and long baselines. We emphasise that these practices are only possible thanks to the narrow transition linewidth in ionic form. In estimating the potential of ion-based nuclear interferometry, we consider the possibility of both terrestrial and space-based experiments, taking guidance from the configurations forecast for the analogous future long-baseline clock atom interferometry experiments based on ^{87}Sr (e.g. AION [53]) in our selection of the relevant experimental parameters.

For the terrestrial setup, we therefore consider a 1 km baseline with $n = 1000$ LMT optics. We set the interferometer separation Δz, to its maximum value

$$\Delta z_{\mathrm{max}} \sim L - v_n T , \qquad (20)$$

where

$$v_n = n \omega_N / m_{\mathrm{Th}} , \qquad (21)$$

is the velocity of the faster half of the wavepacket at the end of the beamsplitter sequence relative to the slower half and m_{Th} denotes the mass of the thorium ion. We select T such that $\Delta z_{\mathrm{max}} \sim L$.

We model our space-based instrument on the design considered in Refs. [43, 50, 104–106], comprising two satellites in medium Earth orbit separated by a distance of 4.4×10^7 m along a single line-of-sight. We take the conservative assumption that the region over which the ions are interrogated is confined to within the interior of the satellites. This constrains the maximum wavepacket separation during the interferometric sequence, $v_n T$, to be less than ~ 1 m [50, 104]. Whilst this inequality is linear in both T and n, we note that due to the dependence of the ion flux and thus the shot-noise spectral density on T, it is preferable to deploy larger n. We select n and T to satisfy this inequality, accounting for the fact that n should be even and that the total duration of the interferometer sequence should exceed the total time

taken for the (sequentially fired) laser pulses to traverse the baseline, i.e. $2T > (4n - 1)L/c$, where c is the speed of light. Whilst the parameters used in our forecasts are representative of the reach that could be attained in such an experiment we note that further optimisation could be performed if one had a particular signal or region of parameter space in mind. Although more ambitious space-based designs in which the interrogation takes place exterior to the satellite allowing for wavepacket separations on the order of ~ 100 m have been proposed [99], this removes the possibility of applying magnetic shielding and would thus leave the ions subject to uncontrollable electric and magnetic fields. This would likely be a major source of gradiometer phase noise which is exacerbated by the large interrogation times associated with this setup[9] and we therefore deem such a design unsuitable and do not consider it further.

For both the terrestrial and space-based designs we set S_{n} to be consistent with Eq. 19, accounting for the fact that one must have both $N_{\mathrm{s}} = 1$ ions per shot and $\Delta t \geq 2T$.

With ions it is also necessary to factor in their enhanced sensitivity to electromagnetic fields. Conventional atom interferometers already have stringent requirements on their internal magnetic environments in order to suppress unwanted contributions to the gradiometer phase which arise from (quadratic) Zeeman shifts to the transition frequency in the presence of temporally or spatially varying magnetic fields. For these interferometers there are two main sources of time-dependent magnetic fields that need to be considered: fluctuations in the local magnetic environment (i.e. for terrestrial interferometers the Earth's magnetic field), and variations in the bias magnetic field which is applied to set a quantisation axis for the atoms and enable the use of magnetically insensitive states for which first order Zeeman shifts are not present. Whilst the use of a bias field is not necessary for nuclear interferometry,[10] fluctuations in the environmental magnetic field remain a potential concern.

The transition frequency of proposed realisations of ionic nuclear clocks is predicted to be significantly more stable to perturbations from external fields than typical atomic optical clocks [59]. Instead, the dominant effect of an external magnetic field on the gradiometer phase arises due to perturbations to the ion's trajectory. For a single interferometer, the leading order phase difference, Φ_i, comes from the acceleration of the interrogated species in the direction of the laser wavevector

---

[9] As will be discussed in due course, the gradiometer phase shift induced by electromagnetic field noise scales with T^2.

[10] As will be discussed, the nuclear transition frequency is predicted to be largely insensitive to perturbations from external fields such that Zeeman shifts are strongly suppressed.

Setup	L [m]	T [s]	n	$\sqrt{S}_{\mathrm{n}}$ [Hz$^{-1/2}$]	Δz [m]
Terrestrial	1000	1.2	1000	2.3	986
Space-based	4.4×10^7	5	16	4.7	4.4×10^7

TABLE I. The experimental parameters characterising the single-ion nuclear interferometers considered in this work: the baseline L, the interrogation time T, the LMT order n, the shot-noise spectral density S_{n}, and the vertical separation Δz between the two interferometers. In the space-based configuration, the interrogation region is taken to be within the interior of the satellites.

(i.e. the z direction): $\Phi_i \sim n\omega_N a_z T^2/c$, where a_z denotes the z-component of the acceleration experienced by the ions and k is the magnitude of the laser wavevector [43, 100, 107]. A magnetic field of magnitude B orientated perpendicularly to the z-axis induces an additional vertical acceleration of $a_z = qBv_t/m_{\mathrm{th}}$ on an ion of charge q and mass m_{th}, where v_t denotes the speed of the particle in the transverse direction perpendicular to the magnetic field. Whilst, in the case of spatially and temporally uniform fields, the phase accrued by each isolated interferometer due to this effect is identical and thus cancels in a differential measurement, spatially dependent magnetic field fluctuations would produce spurious gradiometer phase noise, which, if located in the instrument frequency band, could be indistinguishable from an oscillating ULDM signal.

In particular, if the two interferometers experience a difference in magnetic field of δB in some direction perpendicular to the z axis over the course of the interferometer sequence, an additional gradiometer phase shift of

$$\delta\Phi \sim \left(1\,\mathrm{Hz}^{-\frac{1}{2}}\right)\left(\frac{q}{e}\right)\left(\frac{n}{1000}\right)\left(\frac{v_t}{0.1\mathrm{mm/s}}\right) \times \\ \left(\frac{\delta B}{\mathrm{pT}/\sqrt{\mathrm{Hz}}}\right)\left(\frac{T}{\mathrm{s}}\right)^2 , \quad (22)$$

where $e = 1.6 \times 10^{-19}\,\mathrm{C}$ is the charge of the electron, will be induced. Assuming the transverse velocities of the ions to be $\sim 0.1\,\mathrm{mm/s}$ corresponding to an effective temperature[11] on the order of $\sim$ nK, the terrestrial and space-based configurations detailed in Tab. I remain shot-noise limited for magnetic field fluctuations of amplitude $\delta B \leq 1$ pT$/\sqrt{\mathrm{Hz}}$ and $\delta B \leq 7$ pT$/\sqrt{\mathrm{Hz}}$, respectively. This expression assumes that the time scale over which the field fluctuates is long relative to the interrogation time such that the magnetic field experienced by each interferometer remains approximately constant over the interferometer sequence, which is reasonable for the sub-Hz frequencies and $\mathcal{O}(\mathrm{s})$ interrogation times of relevance here.

It remains to compare these requirements to the magnetic field backgrounds that may be expected for these experiments. At present, the techniques for shielding magnetic fields over the large scales necessary for terrestrial very-long-baseline interferometry (i.e. 10's - 100's of metres) offer screening down to the $\sim$ nT level [109, 110].[12] The amplitudes of stochastic fluctuations in the terrestrial magnetic field at the surface of the Earth in the frequency band of interest are expected to be below these levels [113, 114] and would therefore evade present technologies. Whilst at frequencies exceeding $\sim 1\,\mathrm{Hz}$, the magnitude of these fluctuations is sufficiently small to satisfy the condition for shot-noise domination, they rapidly increase in magnitude below this point [113, 114] such that in the absence of any other means of mitigation, the experiment would become magnetic noise limited with current technology. For the experiment to remain shot-noise limited across the entire operational frequency band, a three order of magnitude improvement in the shielding factor of large scale magnetic shielding would be required. Even without such advances however it may be possible to substantially reduce the impact of magnetic noise through active surveillance and mitigation of the local magnetic environment. To this end, it is possible to measure magnetic fields to sub pT levels with magnetometers. Using an array of such instruments to monitor the local magnetic field strength and direction may allow for a reconstruction of the ion trajectories and the subsequent computation and subtraction of the corresponding gradiometer phase response, as outlined in Ref. [99].

---

[11] Whilst techniques for cooling single trapped ions down to $\sim$ nK thermal temperatures have been proposed [108], we note that transverse velocities of ~ 0.1 mm/s could be realised at higher thermal temperatures by allowing for a greater longitudinal velocity. It is the use of such cooling practices in conventional atom interferometry which have given rise to the use of the notion of 'effective' temperature - the thermal temperature corresponding to the speed in the transverse plane.

[12] Whilst the damping of magnetic field fluctuations and non-uniformities to sub-pT levels has been achieved in certain laboratory settings (see e.g. Ref. [111]), the shielding required for very-long-baseline interferometry is significantly more challenging owing both to the total shield length required [54] and to problems of flux leakage in large length-to-diameter ratio shields [112].

In contrast, temporal fluctuations in the interplanetary magnetic field (as relevant to a space-based instrument) of frequency f at $\sim 1\,\mathrm{AU}$ have been measured to be $\sim 0.1\frac{\mathrm{nT}}{\sqrt{\mathrm{Hz}}} \times \left(\frac{10^{-2}\,\mathrm{Hz}}{f}\right)$ [115]. If these fluctuations could not be shielded or damped, the proposed space-based nuclear interferometer would become limited by magnetic field noise at frequencies below $\sim 0.1\,\mathrm{Hz}$. To this end, retaining shot-noise limited detection over the entire frequency band of the experiment demands either shielding capable of suppressing fluctuations down to the $\sim 7\,\mathrm{pT}$ level across the $\sim 1\,\mathrm{m}$ interrogation region, or a successful active monitoring and mitigation campaign [99]. Given the substantially smaller scales over which fluctuations need to be screened, meeting these shielding demands is likely to prove less challenging than those of the terrestrially-based case.

Gradiometer phase noise can similarly arise from spurious vertical accelerations induced by temporally fluctuating electric fields. Specifically, a difference in the z-component of the electric field experienced by each interferometer of δE generates a gradiometer phase shift of

$$\delta\Phi \sim \left(1\,\mathrm{Hz}^{-\frac{1}{2}}\right)\left(\frac{q}{e}\right)\left(\frac{n}{1000}\right)\left(\frac{\delta E}{0.1\,\mathrm{fVm}^{-1}/\sqrt{\mathrm{Hz}}}\right)\left(\frac{T}{\mathrm{s}}\right)^2 . \tag{23}$$

Remaining in the shot-noise limited regime thus necessitates sufficient shielding of electrostatic fields to keep fluctuations below ~ 0.1 fVm$^{-1}/\sqrt{\mathrm{Hz}}$ and ~ 0.7 fVm$^{-1}/\sqrt{\mathrm{Hz}}$ in the terrestrial and space-based set-ups respectively. These requirements can be be translated to conditions on the metallic vacuum chamber in which these instruments would be housed.

Local patch potentials, spatial and temporal variations of electrostatic potentials across surfaces [116], which are responsible for short-range forces close to surfaces, may pose a further challenge. Given that the dominant way in which electric fields are imprinted in the gradiometer phase comes from perturbations to the z-component of the acceleration of the ions, it is vertical E-fields, as generated from horizontal surfaces which are of greatest concern. In this respect, the ion trajectories (as determined by their launch heights and velocities) should be chosen to keep the ions sufficiently far from the surfaces at the upper and lower ends of the chamber.

B. Neutral Atoms

One could alternatively conceive a nuclear interferometer based upon the ground - isomeric excited state transition in *neutral* ^{229}Th atoms. Whilst this allows for significantly greater effective flux rates and thus much lower

quantum projection noise, there are additional complexities relating to the short lifetime of the excited state which need to be carefully considered. Compared to clock interferometry, in the case of a broad transition the experimental sensitivity is negatively impacted by spontaneous decay occurring both during periods of free propagation in the excited state and during atom-laser interactions. Each of these effects can be accounted for by the introduction of an appropriate correction factor as we shall now detail.

Within an order n single-photon LMT interferometer sequence, the ensembles of atoms are required to spend a total of n periods in the excited state, each lasting for a time $\sim 2L/c$ set by the time for light to travel across the baseline and back. The probability of an atom remaining coherently within the cloud at the end of the sequence is thus (reverting to physical units) [49]

$$P_A = e^{\frac{-2nL}{c\tau}} , \tag{24}$$

where $\tau \sim 7\,\mu\mathrm{s}/\ln(2) \sim 10\,\mu\mathrm{s}$ is the (mean) lifetime of the neutral thorium isomeric excited state [75].

To avoid a significant deterioration of the sensitivity attributed to a given initial number of atoms, the condition

$$nL \leq \frac{c\tau}{2} \sim 1500 \text{ m} , \tag{25}$$

should therefore be satisfied. Unlike single-ions, neutral ^{229}Th is thus restricted to terrestrial scale interferometry experiments.

It is also important to account for the impact of spontaneous decay on the (finite duration) atom-laser interactions. This manifests as a reduction in the efficiency of the so-called π-pulses which are deployed to invert the populations of the ground and excited states. The proposed LMT interferometry scheme depicted in Fig. 1 relies upon a number of π-pulses which are Doppler tuned to selectively interact with a single arm of the interferometer. The velocity resolution of the pulse i.e. the FWHM of the atom velocities which will interact, is

$$\delta v = \frac{\Gamma_a}{\omega_N}\left(1 + \frac{I}{I_{\mathrm{sat}}}\right)^{1/2} , \tag{26}$$

where $\Gamma_a = \tau^{-1}$ is the natural linewidth of the ground-excited isomeric transition in atomic ^{229}Th and the ratio of the applied laser intensity to the transition saturation intensity I/I_{sat}, captures the effect of power broadening. For the laser to successfully interact with a single arm of the interferometer, the velocity separation of the two arms at the time the pulse is applied, Δv, must exceed the velocity resolution. Depending on the location of the pulse within the interferometer sequence, the velocity

separation between the two arms is

$$\Delta v = \frac{\omega_N l}{m_{\mathrm{Th}}} \ , \tag{27}$$

where l takes integer values between 1 and n and represents the difference in the number of times that each of the arms has interacted with the laser. In this instance m_{Th} now denotes the mass of a thorium atom.

The requirement

$$\Delta v > \delta v \ , \tag{28}$$

thus implies a maximum laser intensity

$$\left.\frac{I}{I_{\mathrm{sat}}}\right|_{\mathrm{max},l} = \left(\frac{\omega_N^2 l}{m_{\mathrm{Th}}}\right)^2 - 1 \ . \tag{29}$$

Given that the Rabi frequency, Ω, which sets the duration of the π-pulse according to

$$t_\pi = \frac{\pi}{\Omega} \ , \tag{30}$$

is related to I/I_{sat} by

$$\frac{\Omega^2}{\Gamma_a^2} = \frac{I}{2 I_{\mathrm{sat}}} \ , \tag{31}$$

Eq. 29 therefore implies that there is a minimum π-pulse duration for each l, which, for the transition in question is sizeable relative to the excited state lifetime. Hence it becomes important to account for the impact of spontaneous decay over the duration of the π-pulse. This can be formally achieved by explicitly including spontaneous decay in the optical Bloch equations which describe the behaviour of a 2-level system interacting with an electromagnetic field [117, 118]. The result, which we detail explicitly in Appendix B, is a reduction in the probability that an applied π-pulse results in population inversion from its ideal value of unity according to the value of the ratio Ω/Γ_a.

The interferometer sequence depicted in Fig. 1 involves (4n-3) π-pulses in total, all but 1 of which are intended to selectively interact with a single interferometer arm. Of these, there are 2 pulses which address an $l = 1$ velocity separation, 2 of which act on an $l = n$ velocity separation and a further 4 for each $l \in \{2, ..., n-1\}$. In estimating the total degradation of the sensitivity due to π-pulse inefficiencies over the course of the interferometer sequence, we assume that the laser intensity used for each π-pulse takes its maximum value such that each pulse has as short a duration and thus high as efficiency as possible. In particular we note that for $l = 1$ and $l = 2$ (the only pulse types required for an $n = 2$ LMT

sequence), the minimum pulse durations are achieved at intensity ratios $I/I_{\mathrm{sat}} \sim 25$ and ~ 105 respectively. We additionally assume that the intensity used for the central π-pulse which is designed to simultaneously interact with both arms is sufficiently high such that its duration is negligible with respect to τ. The total probability of having undergone all the desired transitions at the end of the interferometer sequence is then:

$$P_B = P_1^2 P_n^2 \prod_{k=2}^{n-1} P_k^4 \ , \tag{32}$$

where P_k denotes the maximum efficiency of a π-pulse that addresses a single interferometer arm at an $l = k$ velocity separation, obtained by evaluating Eq. B1 at the maximum ratio of Ω/Γ_a according to Eqs. 29 and 31.

Given that the reduction in π-pulse efficiency is sizeable (e.g. $P_1 \sim 0.73$), it is preferable to deploy as few LMT kicks as possible and we thus only consider $n = 2$.[13]

As a result of these two effects, the shot-noise spectrum increases to

$$S_{\mathrm{n}} = \frac{\tilde{S}_{\mathrm{n}}}{P_A P_B} = \frac{e^{\frac{2nL}{c\tau}} \tilde{S}_{\mathrm{n}}}{P_B} \ , \tag{33}$$

where $\widetilde{S}_{\mathrm{n}}$ denotes the noise spectrum for an identical experiment subject to the same initial number of atoms per shot but in the absence of spontaneous decay.

A crucial feature of LMT interferometry is that the atoms propagate in the ground state for the majority of the sequence meaning that it is possible to make use of interrogation times which greatly exceed the excited state lifetime. This has been experimentally demonstrated on table-top scales in Ref. [45] where LMT interferometry was performed on the 689 nm intercombination line of ^{87}Sr.[14] Whilst the short excited state lifetime does not therefore impose a direct upper limit on the duration of the interrogation sequence, the interrogation time does inherit a constraint indirectly from the geometric requirement that the atom trajectories remain within the baseline. This condition implies that for any given choice of L and n there is a maximum T that can be utilised. In practice however, if looking to work in the regime $\Delta z \sim L$, it is necessary to deploy a value of T substantially smaller than this maximum i.e. there is a trade-off between T and Δz which must be accounted for in parameter selection.

----

[13] Note that it is necessary to have $n > 1$ in order that the atoms predominantly propagate in the ground state allowing for interrogation times that exceed the excited state lifetime.

[14] Note that the interferometer sequence deployed in Ref. [45] differs from that proposed in this work, in that every π-pulse is designed to address both arms of the interferometer simultaneously. This is realised by making use of sufficiently high laser intensities such that Eq. 28 is not satisfied.

In our sensitivity forecasts for this scenario, we consider three distinct operating configurations, characterised by the parameters T, L and n, the interferometer separation Δz and the intrinsic phase noise $\sqrt{\tilde{S}_{\mathrm{n}}}$ that arises from the number of atoms launched per shot, representative of an 'initial', 'intermediate' and more 'advanced' experimental design. Whilst we specify our configurations using $\sqrt{\tilde{S}_{\mathrm{n}}}$, we emphasise that it is S_{n}, as defined in Eq. 33, which actually enters the sensitivity calculations in order to account for the additional loss of coherence/atom number due to spontaneous decay. Some justification of these values, which we detail in Tab. II, is in order. As explained above, due to the substantial impact of spontaneous decay on the π-pulse efficiency we are restricted to an $n = 2$ LMT order. According to Eq. 25, the greatest sensitivity will then be reached at a baseline of $\sim 750\,\mathrm{m}$ which we thus deploy for our advanced configuration. In order to take advantage of existing and planned experimental infrastructure, for the initial and intermediate configurations we specifically choose values for L that match the baselines that are, or will be, deployed in the prototype iterations of proposed very-long-baseline clock interferometers based on the ^{87}Sr clock transition.

For $n = 2$, the maximum interferometer separation that can be achieved (assuming equal launch velocities) for a given L and T without the atom trajectories exceeding the baseline is approximately[15]

$$\Delta z_{\max} \sim L - \frac{1}{2}gT^2 \ . \tag{34}$$

Once again we set Δz to $\Delta z_{\max}$ and choose T such that $\Delta z_{\max} \sim L$. We explicitly include the $\Delta z/L$ factor in our sensitivity calculations, noting that this factor becomes increasingly important the shorter the baseline.

As per Eq. 19, in the shot-noise limit the phase sensitivity is essentially controlled at the design level by the time-averaged atomic flux ($N_{\mathrm{s}}/\Delta t$). Given that atom interferometry relies upon the ensemble of atoms being sufficiently cold such that the fraction of atoms that are addressed with each laser pulse is not significantly degraded by the thermal expansion of the cloud over the course of the interferometer sequence, it is laser cooling techniques which ultimately limit the achievable flux rates. As discussed in detail in Refs. [49, 119], the percentage of atoms which interact with each laser pulse follows from a convolution of the spatial and velocity distributions of the ensemble of atoms with the laser pulse Fourier transform and spatial profile of the beam. In our forecasts we assume that the laser beam waist in use is sufficient to address every atom in every interac-

tion. Since the clouds of atoms expand over time as a result of their thermal velocity, the initial temperature to which the atoms are cooled thus needs to be sufficiently low such that the cloud size remains appropriate for the beam waist in use. A greater understanding of the cooling temperatures and laser properties that may be required to achieve this could be developed through a more thorough analysis of the convolution integral. Assuming the usage of a similar beam waist, the requirements on the 3D momentum distribution of an ensemble of thorium atoms are likely to be of similar order of magnitude to those of more typical atom interferometry sources such as strontium (i.e. at the nK - pK level [49, 99]). We thus inform our forecasts of potential fluxes with the initial and more ambitions projections discussed in the context of conventional atom interferometers (see e.g. Ref. [52]).

Whilst it is possible to produce clouds of $10^8 - 10^{10}$ atoms with current techniques [120], the challenge in atom interferometry is to achieve the requisite level of cooling sufficiently rapidly so as to support high shot repetition rates and thus fluxes [99]. The spectral densities of $\sqrt{\tilde{S}_{\mathrm{n}}} = 10^{-4}$, 10^{-5} $(\mathrm{Hz})^{-1/2}$ projected for future long-baseline interferometers such as AION could (theoretically) be realised with 10^8 and 10^{10} uncorrelated atoms per shot at a $1\,\mathrm{Hz}$ shot repetition rate, however are in practice expected to be achieved with fewer atoms and the deployment of squeezing techniques in which the source atoms are entangled [121]. In adopting these flux rates for our forecasts we are thus implicitly assuming the development of the requisite laser cooling and squeezing techniques for ^{229}Th. As is the case for conventional atom interferometers, our projections should therefore be interpreted as indications of the reach that could be achieved in the future should the necessary advancements in cold atom technologies be realised. On comparing our forecasts to those of conventional atom interferometry proposals however, it is important to keep in mind that we have not accounted for any increased experimental challenge that may be associated with cooling and squeezing ^{229}Th as opposed to ^{87}Sr, and therefore that the timescales over which these technologies may be developed are likely to differ.

A second significant challenge of working with neutral ^{229}Th is that the $8.3\,\mathrm{eV}$ nuclear excitation energy is greater than the first ionisation potential of the atom[16] which is $6.3\,\mathrm{eV}$. With the interferometry schemes proposed in this work being reliant on the successful completion of a precise sequence of coherent, laser-induced nuclear excitations and de-excitations, it is necessary to explore the extent to which photo-ionisation would compete with these processes, depleting the number of atoms at the point of detection and reducing the sensi-

---

[15] We emphasise that this approximate expression is valid only for low ($\mathcal{O}(1)$) n.

[16] Note that this is not the case for ionic forms.

Setup	L [m]	T [s]	n	$\sqrt{\tilde{S}_{\mathrm{n}}}$ [Hz$^{-1/2}$]	Δz [m]
Initial	10	0.6	2	10^{-4}	8.2
Intermediate	100	1.8	2	10^{-5}	84
Advanced	750	3.1	2	0.3×10^{-5}	702

TABLE II. The parameters characterising the atom-based nuclear interferometer configurations deployed in the sensitivity forecasts presented in this work. $\sqrt{\tilde{S}_{\mathrm{n}}}$ refers to the 'intrinsic' phase noise set by the shot repetition rate and the number of atoms launched per shot. These values are corrected prior to entering our sensitivity estimates to account for the impact of spontaneous decay as detailed in the main text.

tivity. Whilst a first-principles evaluation of the photo-ionisation and photo-excitation rates of this system lies beyond the scope of this work, we offer a rough preliminary assessment here by comparing estimations of the photo-ionisation and nuclear photo-excitation cross-sections of atomic ^{229}Th in literature.

From the ground electronic configuration, a laser resonant with the isomeric transition is sufficiently energetic to ionise the atom via removal of electrons from either the 6d or 7s electronic shells. At leading order, these processes proceed via allowed (E1) electric dipole transitions. The cross-sections for E1 photo-ionisation of the 6d and 7s electrons are computed numerically in Ref. [122] using the flexible atomic code (FAC) based upon the relativistic configuration interaction method [123]. At an energy of $\sim 8\,\mathrm{eV}$ these cross-sections are of order 10^{-17} cm^2 [122]. In the low saturation limit of moderate laser intensities and a laser bandwidth that exceeds the natural linewidth of the transition, the resonance nuclear photo-excitation cross-section is given by [124]

$$\sigma_{\mathrm{ex.}} \sim \frac{\lambda_0^2}{2\pi} \frac{\Gamma_\gamma}{\Gamma_l} \sim \left(3.6 \times 10^{-20} \right) \times \frac{\Gamma_\gamma}{\Gamma_l} \ \mathrm{cm}^2, \qquad (35)$$

where $\Gamma_\gamma \sim 10^{-9}\ \Gamma_a$ is the radiative decay rate and λ_0 is the transition wavelength. Setting Γ_l to Γ_a, its minimum value consistent with the regime for which this equation is valid, gives $\sigma_{\mathrm{ex.}} \sim 10^{-20}$ cm^2, approximately three orders of magnitude below the photo-ionisation rate. Whilst, as stated in Appendix B, our sensitivity forecasts assume the laser bandwidth to be narrow relative to the natural linewidth to reduce atom loss from spontaneous decay, here we are just interested in an order of magnitude estimate of the nuclear excitation rate in order to assess the extent to which photo-ionisation is likely to be a problem. Given that the nuclear excitation rate should be greatest in the low saturation limit, using this result provides a conservative assessment of the potential impact of photo-ionisation on the interferometry sequence and should thus suffice here.

These preliminary estimates indicate that, unless some means with which to suppress ionisation can be developed, performing interferometry with neutral thorium is unlikely to be feasible due to a significant depletion of the number of atoms remaining coherently in the cloud at detection. Given that the cross-sections of higher order (e.g. first forbidden magnetic dipole M1) ionisation processes are, according to the computations in Ref. [122], approximately 5 orders of magnitude smaller than estimations of the nuclear photo-excitation rate, it should suffice to suppress just the two leading order E1 ionisation channels identified previously. To this end it may be possible to exploit arguments based on transition selection rules to achieve some degree of suppression by working with polarised clouds of atoms and making use of a careful choice of laser polarisation. A number of experimental studies have observed that the total photo-ionisation cross-section of polarised atoms depends on the relative orientation of the atom and laser polarisation (see Refs. [125–128]). However, determining the optimal configuration, in addition to assessing the extent of suppression that may result, demands a full atomic calculation, and falls beyond the remits of this study. It may be that such a practice is insufficient to reach the desired 3 order of magnitude suppression on its own, and that it is necessary to look to other more active methods to achieve this. Various such techniques have been the subject of both theoretical and experimental attention in literature (see Refs. [129–134]) and have been shown capable of suppressing photo-ionisation by several orders of magnitude [135]. The assessment of whether or not such methods (or indeed others) could be adapted to suppress photo-ionisation in ^{229}Th in a way that is compatible with the proposed interferometry sequence lies beyond the scope of this work.

In light of this, in the forecasts presented in Sec. IV of this work we show the reach that could be achieved should it be possible to develop appropriate techniques to suppress photo-ionisation to negligible levels. In this way our estimates serve as motivation from a fundamental physics perspective for a dedicated programme aimed at establishing the feasibility of, and subsequently developing, appropriate atom stabilising technology for ^{229}Th.

Whereas the leading source of noise other than shot-noise affecting the aforementioned single-ion proposal was magnetic field noise, given both the electrical neu-

trality of atoms and the insensitivity of the nuclear clock transition to perturbations from external fields, such fluctuations are much less of a concern here. The attainment of shot-noise limited sensitivity in this case is instead challenged by so-called gravitational gradient noise (GGN)[17] which arises due to mass density fluctuations of the ground and atmosphere around the experiment [136, 137]. These fluctuations perturb the local gravitational potential experienced by the clouds of atoms, generating spurious gradiometer phase shifts. This type of noise cannot be shielded and has been identified as a major challenge for conventional terrestrial very-long-baseline atom interferometry proposals [52]. For typical 100 m- and km-scale instruments, GGN is to expected surpass the shot-noise at $\sim$ sub-Hz frequencies, leading to a significant loss of sensitivity [101, 138–141].

The modelling and mitigation of GGN at terrestrial atom interferometers constitutes an active and involved area of research (see e.g. Ref. [141]) which depends both on details of the interferometry sequence and the local seismic environment of the experiment. Given this latter consideration, we do not attempt to perform any first-principles calculations here, but instead estimate the potential impact of GGN on the atom-based nuclear interferometer designs specified in Tab. II by adapting existing analyses for standard long-baseline atom interferometers presented in the literature to account for differences in the interferometry sequence and instrument design.

The GGN spectral density for both a 100 m- and a km-scale atom interferometer with the design specifications detailed in Tab. III were calculated in Ref. [141] in the $10^{-3} - 10$ Hz frequency band by modelling the seismic field as an incoherent superposition of monochromatic plane waves propagating isotropically at the Earth's surface. Results for both a representative low and high noise seismic environment were presented, based respectively on the empirically driven Peterson new low and high noise models [142].

At low frequencies, the GGN spectral noise density, S_{ggn}, scales approximately with the interferometer design parameters as $\sim n^2 L^2 T^4$ [141]. To obtain a conservative estimate the impact of GGN on the nuclear interferometer configurations considered in this work, we re-scale the high noise S_{ggn} presented in Ref. [141] according to the parameters of our instruments and locate the frequency at which this becomes dominant over the shot-noise.[18] Due to both the substantially lower n and the increased

shot-noise (due to the corrections for spontaneous decay) of the intermediate and advanced nuclear interferometer designs proposed here, we find that they remain shot-noise limited down to lower frequencies: $\sim 10^{-3}$ Hz and $\sim 10^{-2}$ Hz respectively, compared to the $\sim$ Hz threshold of the 100 m and km instruments of Tab III.

The analysis of Ref. [141] found that the sensitivity of the 10 m instrument defined in Tab. III was not impacted by GGN in the frequency band considered in either the low or high noise scenarios. It is therefore safe to assume that our 10 m initial nuclear interferometer would also remain in the shot-noise limited regime above 10^{-3} Hz, however a full calculation of the GGN spectral density at lower frequencies would be required to obtain a more precise handle on the frequency down to which this is the case. For this reason, when we delineate the frequencies at which different instruments may become GGN-limited on our plots in Sec. IV, we conservatively take a 10^{-3} Hz threshold for the 10 m instruments of both Tab. II and Tab. III.

Given the potential impact of GGN at terrestrial atom interferometers, various passive mitigation techniques, which may also be applicable to nuclear interferometry, are under active investigation. In particular it was shown in Ref. [141] that multigradiometer configurations in which multiple interferometers are positioned along the same baseline, could greatly reduce the impact of GGN on ULDM searches and recover significant regions of parameter space accessible to shot-noise limited instruments. A carefully selected site location with a quiet seismic environment (i.e. approaching the Peterson low noise as opposed to high noise model) may also offer the opportunity to regain up to three orders of magnitude in sensitivity [52].

IV. DISCUSSION

In Figs. 2, 3 and 4, we plot the couplings d_e, d_g and $d_{\hat{m}}$ that could be detected at a signal-to-noise ratio (SNR) of 1 with the single-ion interferometer designs specified in Tab. I following a measurement period of $T_{\text{int}} = 10^8$ s, assuming that the coupling in question dominates d_ϕ. In Figs. 5, 6 and 7, we present the shot-noise limited reach of the neutral atomic interferometer configurations of Tab. II, once again taking $T_{\text{int}} = 10^8$ s and assuming the suppression of photo-ionisation to negligible levels. For clarity, our plots show the power-averaged envelope of the experimental response using the approximation $\sin x = \min(x, 1/\sqrt{2})$ as in Ref. [40].

We emphasise that our forecasts assume the nuclear interferometer sensitivity to be shot-noise limited over the entire frequency band of the experiment. As dis-

---

[17] Whilst GGN similarly affects the ionic proposal previously discussed, it is substantially smaller than the high shot-noise resulting from single ion shots and thus does not limit the sensitivity.

[18] We emphasise that it is S_n, the shot-noise spectral density accounting for spontaneous decay which should be used for this comparison.
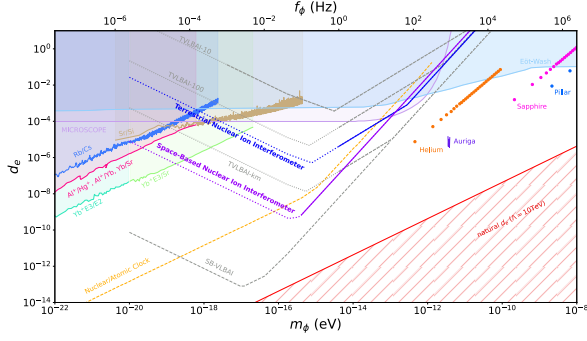
FIG. 2. Shot-noise limited projected sensitivity of the single-ion nuclear interferometer configurations detailed in Tab. I to ULDM with a linear scalar coupling to photons. The curves show the minimum coupling d_e that could be detected at a SNR = 1 following an experimental campaign of duration $T_{\rm int} = 10^8$s. The dotted portion of the curve indicates where the sensitivity may be adversely impacted by magnetic field noise according to the discussion in Sec. III. Also shown are existing bounds and forecast sensitivities of other experiments as detailed in the main text. The parameter space motivated from a naturalness perspective as described in the text is shown in red.

FIG. 3. Same as Fig. 2 but for ULDM with a linear scalar coupling to gluons.
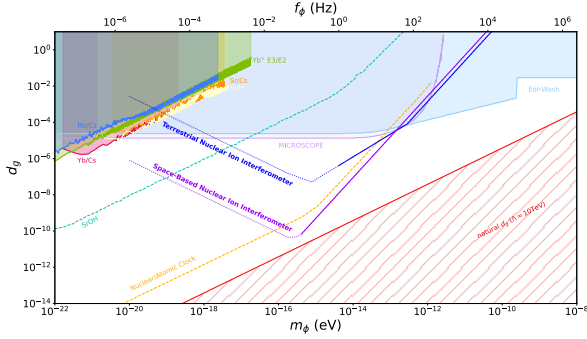
FIG. 4. Same as Fig. 2 but for ULDM with a linear scalar coupling to quarks.

cussed in Sec. III, there may however be other sizeable noise sources which could become dominant. In order to reflect this, we indicate on our plots the frequencies, as determined by the analysis in Sec. III, at which the experiment may depart from the shot-noise limited regime due to either magnetic field noise (in the case of ions) or GGN (in the case of atoms) with the use of a dotted, as opposed to a solid, line. We highlight that these thresholds assume that no attempts to mitigate either noise source either actively or passively are made. Advancements in large-scale magnetic shielding technology, a well-chosen site location and close environmental monitoring could all help to extend the shot-noise limited regime into lower frequencies and to recover regions of the impacted parameter space.
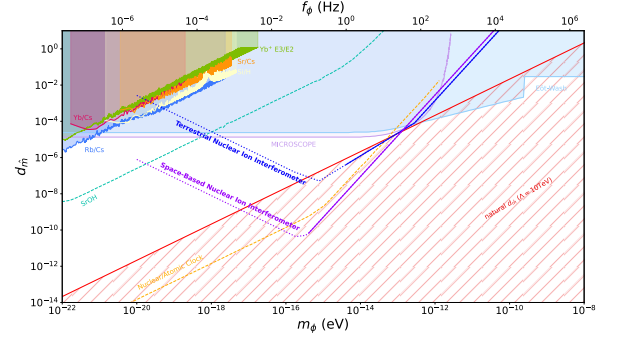
For context, also shown in these figures are the 95% confidence level (CL) limits on the considered couplings from tests of the Equivalence Principle (EP) both with Eöt-Wash torsion balance experiments [143, 144] and MICROSCOPE [145, 146], as computed in Ref. [147]. We also display the limits from a hyperfine frequency comparison of rubidium and caesium (Rb/Cs) atomic microwave clocks [148], in addition to the estimated reach of a frequency comparison between the ^{229}Th nuclear clock and an atomic optical clock [5, 29]. Upon the recommendation of Ref. [90], the Rb/Cs limits derived in Ref. [148] have been rescaled by a factor of 3 in order to properly account for the stochastic nature of the scalar ULDM field and enable consistent comparison with competing bounds and proposals.

In the case of the coupling to photons d_e, we also show limits from the AURIGA detector [149], the frequency comparison of the electric octupole and the electric quadrupole clock transitions in single-ion ytterbium (Yb$^+$ E3/E2), the comparison of the Yb$^+$ E3 transition to the strontium $S \rightarrow P$ clock transition (Yb$^+$ E3/Sr) [37], the comparison of a strontium optical clock with a silicon cavity (Sr/Si) [150] and the combined constraints of several optical clock comparisons (Al$^+$/Hg$^+$, Al$^+$/Yb, Yb/Sr) from the Boulder atomic clock optical network [36]. Forecasts for the sensitivities of proposed compact mechanical resonators based on superfluid helium, sapphire cylinders and sapphire pillars [34] are also shown, as are the prospective shot-noise limited sensitivities of very-long-baseline atom interferometers operating on the ^{87}Sr atomic clock transition. We show forecasts for terrestrial configurations (TVLBAIs) with 10 m, 100 m and 1 km scale baselines in addition to a potential space-based realisation (SB-VLBAI), assuming the experimental parameters listed in Tab. III. Further details on the calculation of these estimates, including a justification of the parameters used, can be found in Appendix C. As for the atom-based nuclear interferometers we indicate the frequencies at which the sensitivities of these experiments are likely to be impacted by GGN, assuming both a high

seismic environment and that no mitigation strategies are applied, according to the analysis in Ref. [141], by switching from a dashed to a dotted line.

In the case of the couplings to quarks and gluons, we show bounds from the comparison of a Yb lattice clock with a caesium fountain microwave clock (Yb/Cs) [151], the comparison of strontium and caesium clocks (Sr/Cs) [152], the comparison of a hydrogen maser with a silicon cavity [150] and the comparison of the E3/E2 transitions in Yb$^+$ [153]. Whilst the first three of these comparisons involve a microwave hyperfine transition, in the latter, the sensitivity to d_g and $d_{\hat{m}}$ derives from ULDM-induced oscillations of the nuclear charge radius. Also shown are projections for the comparison of a molecular SrOH clock with an atomic optical clock, assuming a total data accumulation period of 1 year [154].

We emphasise that whilst a variety of other experiments have probed, or have been proposed to probe each of these couplings, for clarity and efficiency, we have shown here just a representative selection of those which yield the strongest bounds or greatest prospective sensitivities in the parameter space of relevance. A more detailed overview of the landscape of competing experiments can be found (e.g. for d_e) in Ref. [5].

The red shading in each of these figures delineates the parameter space which is motivated from a naturalness perspective. We derive this following Ref. [40]. The central argument here is that these scalar interactions break any shift symmetry which could keep the scalar light, such that a mass-squared contribution is expected from within the UV theory, scaling as the square of the coupling. Motivated by the scales already explored by the LHC, we conservatively take the cutoff of the IR (infrared/ low-energy) theory at which these UV-contributions are predominantly generated to be 10 TeV and determine the parameter space in which these generic UV contributions are smaller than the scalar mass, thus avoiding the requirement of fine-tuning of different UV contributions to arrive at a given scalar mass, given a certain scalar coupling.

It is important to realise that whilst the bounds from tests of the EP are independent of the abundance of ϕ, the other experiments shown on these plots, including our forecasts for the various nuclear interferometer realisations, implicitly assume ϕ to comprise the totality of the relic local DM abundance. At low masses $m_\phi < 2 \times 10^{-20}$ eV, this scenario has been ruled out by examination of small-scale cosmological structure in the Lyman-α forest [155].

Together, these figures illustrate the discovery reach of nuclear interferometry, with the potential to open windows to large regions of currently uncharted phenomenological territory, thus facilitating a broader exploration
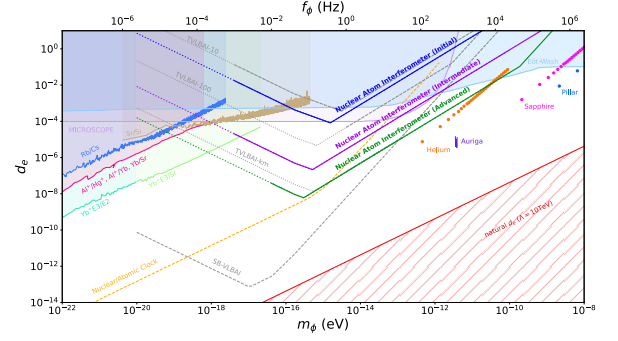

FIG. 5. Shot-noise limited projected sensitivity of the nuclear interferometer configurations deploying neutral atoms detailed in Tab. II to ULDM with a linear scalar coupling to photons. The curves show the minimum coupling d_e that could be detected at a SNR = 1 following an experimental campaign of duration $T_{\text{int}} = 10^8$ s and assuming that photo-ionisation has been successfully suppressed. The dotted portion of the curve indicates where the sensitivity may be adversely impacted by GGN according to the discussion in Sec. III. Also shown are existing bounds and forecast sensitivities of other experiments as detailed in the main text. The parameter space motivated from a naturalness perspective as described in the text is shown in red.
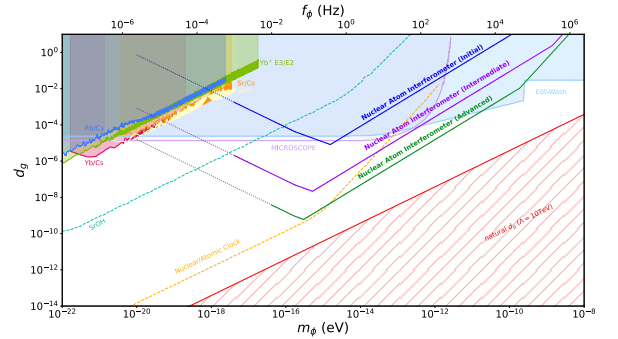

FIG. 6. Same as Fig. 5 but for ULDM with a linear scalar coupling to gluons.
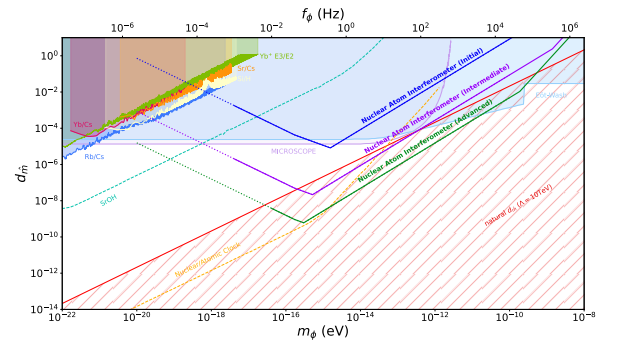

FIG. 7. Same as Fig. 5 but for ULDM with a linear scalar coupling to quarks.

of the dark matter landscape. As a result of their differing operating conditions, the ionic and atomic nuclear interferometer realisations proposed in this work naturally target contrasting regions of parameter space and are thus complementary in their potential physics gain. Whilst the single-ion nuclear interferometer may, if operated in space, be able to achieve significantly greater peak sensitivities than an instrument deploying clouds of neutral ^{229}Th, the experimental parameters required for this latter realisation naturally favour higher mass particles with a significantly shallower degradation of sensitivity moving in the direction of increasing ULDM mass.

In Figs. 2 and 5, we respectively show the reach of a single-ion and a neutral atom nuclear interferometer to ULDM coupling to photons, whose future experimental landscape is expected to be most strongly constrained by long-baseline ^{87}Sr atomic clock interferometers and nuclear-atomic optical clock comparisons. Due to the intrinsically limited ion flux, we find that terrestrial single-ion nuclear interferometers are unable to fully benefit from the increased sensitivity of the nuclear clock transition to the variation of fundamental constants, and are likely to be out-performed by conventional ^{87}Sr-based terrestrial interferometers, provided that the target atomic fluxes (as listed in Tab. III) can be reached. Much higher sensitivities could be achieved in space-based experiments with the substantial increase in baseline afforded by such realisations compensating for the high shot-noise associated with working with single ions.

In contrast, we find that the ~ 4 order of magnitude increase in sensitivity of the ground-excited isomeric state transition to the variation of d_e compared to standard atomic optical clocks is sufficient to overcome challenges associated with the short excited state lifetime in neutral ^{229}Th, rendering terrestrial atom-based nuclear interferometers competitive with their ^{87}Sr clock analogues in addition to improving their reach at higher masses. Beyond that, such enhancements can be achieved with both significantly less demanding LMT requirements and more modest baselines (as is indeed required due to the short excited isomeric lifetime), than are necessary to deploy in conventional atom interferometry.

The potential of nuclear interferometry to advance existing experimental proposals is substantially greater in searches for new physics coupling to the QCD sector via the couplings d_g and $d_{\hat{m}}$, as displayed in Figs. 3, 4, 6 and 7. These couplings enter the frequencies of typical atomic optical clock transitions via the ratio of the electron mass to the nucleus mass (m_e/m_{nuc}) in the reduced mass of the system, rendering their contribution suppressed by approximately 5 orders of magnitude with respect to that of d_e. As such, the sensitivity of conventional atomic clock interferometers to such effects is not appreciable and for consistency with literature is not shown in these

figures. We note that in Ref. [153] it was shown that in heavy-nucleus optical clocks such as ^{171}Yb$^+$, the transition frequency becomes sensitive to the nuclear-charge radius, leading to an enhanced sensitivity to the couplings d_g and $d_{\hat{m}}$ by ~ 2 orders of magnitude. Such systems could in principle be deployed in clock atom interferometry experiments as recently suggested in Ref. [156] where oscillations of the nuclear charge radius in a space-based atom interferometry experiment using a (neutral) Yb source were considered. We emphasise that the intrinsic sensitivity of this transition to variations of d_g and $d_{\hat{m}}$ is still many orders of magnitude below that of the nuclear clock however.

We highlight that the deployment of the nuclear clock in an interferometry-based search for ULDM as proposed in this work is complementary to its usage in nuclear-atomic optical clock frequency comparison experiments. Indeed, as can be seen in the plots, the nuclear interferometer pushes the potential parameter space coverage closer to, and in the case of $d_{\hat{m}}$ into, more theoretically motivated regions where the couplings can be deemed technically natural.

The entirety of the discussion up to this point has been based on operating the interferometer in 'broadband' mode. In principle, one could alternatively operate in 'resonant' mode [104] in which the interferometer space-time diagram comprises Q closed diamonds each of duration $2T$. This results in a Q-factor sensitivity enhancement to the mass $m_\phi = \pi/T$ over a mass range $\pi/(QT)$ relative to a broadband search with the same experimental parameters. Such schemes are, in the context of conventional atom interferometers, thought to be of particular benefit to space-based designs in which the atom interrogation is confined to the interior of the satellites, greatly restricting the LMT order n that can be employed [50, 104]. With the on-resonance sensitivity scaling linearly with both Q and n in resonant mode (see Ref. [92]), it is possible to exploit the parameter Q whilst maintaining a sufficiently low n so as to adhere to the geometric constraints in order to reach considerably greater sensitivities than could be achieved with broadband operation. In Ref. [40], it was shown that systematically scanning through a band of resonant masses over the course of the experimental campaign by altering Q and T could extend the reach of space-based ^{87}Sr interferometers to masses in this band relative to the equivalent broadband search. Given that resonant mode operation involves an increased number of atom-laser interactions, for the atom-based nuclear interferometer the low π-pulse efficiencies mean such schemes are unlikely to be of any benefit. In contrast, for ion-based interferometers we do expect a scanned resonant search to yield increased sensitivities, particularly to masses at the higher end of the band. Due to the dependence of the shot-noise on the total duration of the interferometer sequence, which in resonant mode is increased by a factor Q to $2QT$, the rel-

ative enhancement over the analogous broadband search will not be as significant as that which may be achieved for ^{87}Sr atom interferometers however.

Though not studied in this work, we highlight that the nuclear interferometer is not limited to investigating ULDM with scalar couplings. In particular, the pseudo-scalar coupling of axions and axion-like particles to gluons induces oscillations in the thorium transition energy at quadratic order in the axion field [157] and would thus generate a signal in a nuclear interferometer. We leave a more detailed treatment of this scenario to future work.

Whilst the reach of the proposals presented here remains limited by the high shot-noise and the short lifetime of the excited state respectively, this work demonstrates that there is nonetheless the potential, provided experimental challenges can be overcome in the future, to access new, previously uncharted, phenomenological territory with the nuclear interferometer. Not only does this serve as testament to the unique and exciting role that ^{229}Th may play in our future explorations of new physics, but it motivates a closer investigation of its potential within the field of long-baseline interferometry. For example, in the case of single-ions, one might explore different interferometer geometries to enable the use of greater ion fluxes, and in neutral atoms, alternative interferometry schemes deploying floquet atom optics [158] could be considered as a means to achieve higher π-pulse efficiencies.

A further interesting line of enquiry could be to investigate the possibility of binding ^{229}Th into a molecule. Not only would it be necessary to verify that the nuclear transition, and its enhanced sensitivity to the variation of fundamental constants remains intact in such a system, but that both the dissociation and ionisation energies of the molecules lie above the nuclear transition energy. To fully harness the benefits that working with a neutral species presents in terms of the shot-noise, it would be desirable for the excited nuclear state to be long lived, avoiding the complications associated with spontaneous decay seen in the atomic case.

V. CONCLUSIONS

With an extraordinarily broad landscape of viable candidates which give rise to a diverse range of phenomenological signatures, new ideas for the detection of DM are required in order to maximise experimental coverage of the vast available parameter space. In this work we propose two possible realisations of a single-photon interferometry experiment based on the nuclear clock transition in ^{229}Th as a probe of ULDM with scalar couplings to the SM, making use of single-ions and clouds of neutral

atoms respectively. Although working with either source type presents a unique set of experimental challenges, we find that the enhanced sensitivity of the nuclear clock transition to the variation of fundamental constants offers the means to access large regions of uncharted parameter space over a wide range of frequencies providing experimental challenges can be met in the future.

In particular, nuclear interferometry could offer a unique opportunity to probe scalar couplings of ULDM to gluons and quarks, with a sensitivity exceeding existing and proposed experiments over a range of frequencies. Employing the nuclear clock in this way complements its usage in nuclear-atomic optical clock frequency comparisons, with the peak sensitivity moving towards more theoretically motivated regions of parameter space. Although by no-means fully optimised, this proposal highlights the important role which ^{229}Th could play in future searches for new physics, motivating a broader investigation into its potential capabilities both within interferometry and beyond.

Appendix A: Sensitivity to ULDM Couplings

Here we briefly outline how the experimental sensitivity given in Eq. 18 follows from Eq. 15, the signal amplitude for a single measurement.

The experimental sensitivity takes into account a total of N phase measurements made continuously at a regular sampling rate $1/\Delta t$ over the experiment run time T_{int}. We denote these measurements as $\{\Phi_m\}$, where m labels the phase recorded from the interferometer sequence starting at time $m\Delta t$.

A discrete set of measurements made at different times can be conveniently characterised by its power spectral density (PSD), which contains information on both the amplitude and the frequency spread of the data. The PSD can be constructed via the Fourier transform of the measured signal

$$\tilde{\Phi}_k = \sum_{m=0}^{N-1} \Phi_m \exp\left(-\frac{2\pi i m k}{N}\right) , \qquad (A1)$$

where k takes integer values between 0 and $N-1$.

Using this definition, the PSD, S_k, can be expressed as

$$S_k = \frac{(\Delta t)^2}{T_{\text{int}}} \left|\tilde{\Phi}_k\right|^2 . \qquad (A2)$$

Defining the angular frequency as $\omega = 2\pi k/T_{\text{int}}$, in the limit of shot-noise domination, the SNR at a frequency ω_0 is then given by

$$\text{SNR} = \frac{S_{\text{s}}(\omega_0)}{S_{\text{n}}(\omega_0)} , \qquad (A3)$$

where $S_{\text{s}}(\omega)$ denotes the PSD of the ULDM induced signal and $S_{\text{n}}(\omega)$ denotes the shot-noise PSD as given by Eq. 19.

In the limit $T_{\text{int}} < \tau_c$, the ULDM signal is dominated by a single frequency such that the signal PSD takes the form

$$S_s(\omega) \sim \begin{cases} T_{\text{int}}|\overline{\Phi}_s|^2, & \omega = \omega_0 \\ 0, & \omega \neq \omega_0 \end{cases} . \qquad (A4)$$

The experimental sensitivity to these couplings in this regime is thus

$$d_\phi \simeq \frac{\sqrt{\text{SNR}}}{\overline{\Phi}_R} \times \sqrt{\frac{S_{\text{n}}}{T_{\text{int}}}} . \qquad (A5)$$

If instead $T_{\text{int}} > \tau_c$, the signal PSD has a finite profile in frequency space determined by the DM velocity distribution. In this instance, the experimental sensitivity can be computed using Bartlett's method [92, 159, 160], leading to

$$d_\phi \simeq \frac{\sqrt{\text{SNR}}}{\overline{\Phi}_R} \times \sqrt{\frac{S_{\text{n}}}{\sqrt{\tau_c T_{\text{int}}}}} . \qquad (A6)$$

Combining these two results leads directly to Eq. 18.

Appendix B: π-pulse efficiencies

The behaviour of a 2-level atomic or nuclear system coherently interacting with an external electromagnetic field (i.e. a laser) over time can be described by the optical Bloch equations (see e.g. Refs. [117, 118]). These equations model the time evolution of a density operator $\hat{\rho}$ which encodes the occupation probabilities of the ground and excited states. When the field is on resonance with the transition, in the absence of spontaneous decay, the population probabilities of the ground and excited state oscillate at the so-called Rabi frequency, Ω, such that after a time $t_\pi = \pi/\Omega$, a system initialised in the ground state has a 100% probability of having transitioned to the excited state. Pulses of this duration are commonly referred to as π-pulses, and as discussed in the main text, play a crucial role in the coherent transfer of populations in matter-wave interferometry.

To estimate the π-pulse efficiency in the presence of spontaneous decay, one can explicitly introduce spontaneous decay to the optical Bloch equations and solve for the probability of being in the excited state as a function of time assuming that the system is initialised in the ground state and that the electromagnetic field (i.e. the laser) is resonant with the transition. This calculation, which can be performed analytically, is sometimes known as Torrey's solution [161] and is derived in full in Refs. [117, 162]. For a comprehensive discussion of these equations in the context of nuclear transitions, we refer the reader to Ref. [124].

Evaluating the excited state probability at $t_\pi = \pi/\Omega$ yields

$$P\Big|_{t=t_\pi} = \frac{\Omega^2}{2\Omega^2 + \Gamma_a^2} \times$$
$$\left[1 - e^{-\frac{3\Gamma_a \pi}{4\Omega}} \left[\cos\left(\frac{\Omega_\Gamma}{\Omega}\pi\right) + \frac{3\Gamma_a}{4\Omega_\Gamma} \sin\left(\frac{\Omega_\Gamma}{\Omega}\pi\right)\right]\right] , \qquad (B1)$$

where

$$\Omega_\Gamma = \Omega\sqrt{1 - \left(\frac{\Gamma_a}{4\Omega}\right)^2} . \qquad (B2)$$

In quoting this result we have implicitly taken the limit that the bandwidth of the exciting laser, Γ_l, is significantly less than the natural width of the transition $\Gamma_a \sim 16$ kHz, such that the rate of decoherence in the optical Bloch equations: $\tilde{\Gamma} = (\Gamma_a + \Gamma_l)/2$ is entirely due to spontaneous decay i.e. $\tilde{\Gamma} \sim \Gamma_a/2$. It is this regime which maximises the π-pulse efficiency.

We take Eq. B1 - i.e. the probability that a pulse of duration t_π results in a population inversion - to be the π-pulse efficiency that we use in making our sensitivity forecasts and emphasise that it is entirely governed by the ratio Ω/Γ_a.

Appendix C: AION Prospective Sensitivity

The sensitivity curves labelled TVLBAI-10, TVLBAI-100 and TVLBAI-km displayed in Fig. 5 refer specifically to terrestrial atom interferometers operating on the 698 nm $5s^2\ ^1S_0 \leftrightarrow 5s5p\ ^3P_0$ clock transition in ^{87}Sr assuming the experimental parameters detailed in Tab. III. These choices match those that may be implemented in future vertical atom gradiometers such as AION. In particular, the TVLBAI-km parameters correspond to those used in the plots presented by the terrestrial very-long-baseline atom interferometry community in Ref. [52]. The TVLBAI-10 and TVLBAI-100 parameter sets match configurations considered by the AION collaboration in Refs. [92] and [53] respectively. The parameters chosen for the SB-VLBAI configuration are appropriate for a broadband search at AEDGE with the interrogation region situated exterior to the satellites. In this respect the values of n and T are selected to achieve a maximum cloud separation of ~ 100 m whilst paying heed to the constraints on the maximum number of laser pulses (1000) and the maximum interferometer sequence duration (300 s) that could be implemented at AEDGE as stated in Ref. [106]. For each of these forecasts, a total campaign duration of 10^8 s is assumed.

The projections are calculated using Eq. 15 but with $\overline{\Delta\omega}_N$ replaced by

$$\overline{\Delta\omega}_A = \omega_A \kappa \phi_0 \left(2 + \xi_A\right) d_e \ , \tag{C1}$$

where $\omega_A = 1.78$ eV [163] and $\xi_A \sim 0.06$ [164].

[1] M. Battaglieri et al., *US Cosmic Visions: New Ideas in Dark Matter 2017: Community Report*, in *U.S. Cosmic Visions: New Ideas in Dark Matter*, 7, 2017, 1707.04591.

[2] A. M. Green and B. J. Kavanagh, *Primordial Black Holes as a dark matter candidate*, *J. Phys. G* **48** (2021) 043001, [2007.10722].

[3] Particle Data Group collaboration, R. L. Workman et al., *Review of Particle Physics*, *PTEP* **2022** (2022) 083C01.

[4] J. Jaeckel and A. Ringwald, *The Low-Energy Frontier of Particle Physics*, *Ann. Rev. Nucl. Part. Sci.* **60** (2010) 405–437, [1002.0329].

[5] D. Antypas et al., *New Horizons: Scalar and Vector Ultralight Dark Matter*, 2203.14915.

[6] R. D. Peccei and H. R. Quinn, *CP Conservation in the Presence of Instantons*, *Phys. Rev. Lett.* **38** (1977) 1440–1443.

[7] M. A. Shifman, A. I. Vainshtein and V. I. Zakharov, *Can Confinement Ensure Natural CP Invariance of Strong Interactions?*, *Nucl. Phys. B* **166** (1980) 493–506.

[8] L. Di Luzio, M. Giannotti, E. Nardi and L. Visinelli, *The landscape of QCD axion models*, *Phys. Rept.* **870** (2020) 1–117, [2003.01100].

[9] B. Holdom, *Two U(1)'s and Epsilon Charge Shifts*, *Phys. Lett. B* **166** (1986) 196–198.

[10] P. Fayet, *Extra U(1)'s and New Forces*, *Nucl. Phys. B* **347** (1990) 743–768.

[11] M. Fabbrichesi, E. Gabrielli and G. Lanfranchi, *The Dark Photon*, 2005.01515.

[12] S. Dimopoulos and G. F. Giudice, *Macroscopic forces from supersymmetry*, *Phys. Lett. B* **379** (1996) 105–114, [hep-ph/9602350].

[13] N. Arkani-Hamed, L. J. Hall, D. Tucker-Smith and N. Weiner, *Solving the hierarchy problem with exponentially large dimensions*, *Phys. Rev. D* **62** (2000) 105002, [hep-ph/9912453].

[14] C. P. Burgess, A. Maharana and F. Quevedo, *Uber-naturalness: unexpectedly light scalars from supersymmetric extra dimensions*, *JHEP* **05** (2011) 010, [1005.1199].

[15] M. Cicoli, C. P. Burgess and F. Quevedo, *Anisotropic Modulus Stabilisation: Strings at LHC Scales with Micron-sized Extra Dimensions*, *JHEP* **10** (2011) 119, [1105.2107].

[16] T. Damour and A. M. Polyakov, *The String dilaton and a least coupling principle*, *Nucl. Phys. B* **423** (1994) 532–558, [hep-th/9401069].

[17] T. R. Taylor and G. Veneziano, *Dilaton Couplings at Large Distances*, *Phys. Lett. B* **213** (1988) 450–454.

[18] F. Piazza and M. Pospelov, *Sub-eV scalar dark matter through the super-renormalizable Higgs portal*, *Phys. Rev. D* **82** (2010) 043533, [1003.2313].

[19] P. W. Graham, D. E. Kaplan and S. Rajendran, *Cosmological Relaxation of the Electroweak Scale*, *Phys. Rev. Lett.* **115** (2015) 221801, [1504.07551].

[20] A. Banerjee, H. Kim and G. Perez, *Coherent relaxion dark matter*, *Phys. Rev. D* **100** (2019) 115026, [1810.01889].

[21] E. G. M. Ferreira, *Ultra-light dark matter*, *Astron. Astrophys. Rev.* **29** (2021) 7, [2005.03254].

[22] L. Hui, *Wave Dark Matter*, *Ann. Rev. Astron. Astrophys.* **59** (2021) 247–289, [2101.11735].

Setup	L (m)	T (s)	n	$\sqrt{S_n}$ (Hz$^{-1/2}$)	Δz (m)
TVLBAI-10	10	0.3	1000	10^{-4}	7.8
TVLBAI-100	100	1.4	1000	10^{-4}	90
TVLBAI-km	1000	1.7	2500	10^{-5}	970
SB-VLBAI	4.4×10^7	100	150	10^{-5}	4.4×10^7

TABLE III. The parameters used in the ^{87}Sr source terrestrial and space-based very-long-baseline atom interferometer sensitivity curves displayed in Fig. 2 and Fig. 5. These values correspond to configurations considered by proposed long-baseline atom interferometry experiments as detailed in the text.

[23] M. S. Safronova and D. Budker, *Quantum technologies and the elephants*, *Quantum Science and Technology* **6** (aug, 2021) 040401.

[24] M. S. Safronova, D. Budker, D. DeMille, D. F. J. Kimball, A. Derevianko and C. W. Clark, *Search for New Physics with Atoms and Molecules*, *Rev. Mod. Phys.* **90** (2018) 025008, [1710.01833].

[25] O. Buchmueller et al., *Snowmass 2021: Quantum Sensors for HEP Science – Interferometers, Mechanics, Traps, and Clocks*, in *Snowmass 2021*, 3, 2022, 2203.07250.

[26] A. Chou et al., *Quantum Sensors for High Energy Physics*, in *Quantum Sensors for HEP workshop report*, 11, 2023, 2311.01930.

[27] S. D. Bass and M. Doser, *Quantum sensing for particle physics*, 2305.11518.

[28] J.-P. Uzan, *Varying Constants, Gravitation and Cosmology*, *Living Rev. Rel.* **14** (2011) 2, [1009.5514].

[29] A. Arvanitaki, J. Huang and K. Van Tilburg, *Searching for dilaton dark matter with atomic clocks*, *Phys. Rev. D* **91** (2015) 015015, [1405.2925].

[30] Y. V. Stadnik and V. V. Flambaum, *Searching for dark matter and variation of fundamental constants with laser and maser interferometry*, *Phys. Rev. Lett.* **114** (2015) 161301, [1412.7801].

[31] Y. V. Stadnik and V. V. Flambaum, *Can dark matter induce cosmological evolution of the fundamental constants of Nature?*, *Phys. Rev. Lett.* **115** (2015) 201301, [1503.08540].

[32] P. W. Graham, D. E. Kaplan, J. Mardon, S. Rajendran and W. A. Terrano, *Dark matter direct detection with accelerometers*, *Phys. Rev. D* **93** (Apr, 2016) 075029.

[33] A. A. Geraci, C. Bradley, D. Gao, J. Weinstein and A. Derevianko, *Searching for ultralight dark matter with optical cavities*, *Phys. Rev. Lett.* **123** (Jul, 2019) 031304.

[34] J. Manley, D. Wilson, R. Stump, D. Grin and S. Singh, *Searching for Scalar Dark Matter with Compact Mechanical Resonators*, *Phys. Rev. Lett.* **124** (2020) 151301, [1910.07574].

[35] D. Carney et al., *Mechanical Quantum Sensing in the Search for Dark Matter*, *Quantum Sci. Technol.* **6** (2021) 024002, [2008.06074].

[36] BACON collaboration, K. Beloy et al., *Frequency ratio measurements at 18-digit accuracy using an optical clock network*, *Nature* **591** (2021) 564–569, [2005.14694].

[37] M. Filzinger, S. Dörscher, R. Lange, J. Klose, M. Steinel, E. Benkler et al., *Improved Limits on the Coupling of Ultralight Bosonic Dark Matter to Photons from Optical Atomic Clock Comparisons*, *Phys. Rev. Lett.* **130** (2023) 253001, [2301.03433].

[38] E. Madge, G. Perez and Z. Meir, *Prospects of nuclear-coupled-dark-matter detection via correlation spectroscopy of I2+ and Ca+*, *Phys. Rev. D* **110** (2024) 015008, [2404.00616].

[39] A. A. Geraci and A. Derevianko, *Sensitivity of atom interferometry to ultralight scalar field dark matter*, *Phys. Rev. Lett.* **117** (2016) 261301, [1605.04048].

[40] A. Arvanitaki, P. W. Graham, J. M. Hogan, S. Rajendran and K. Van Tilburg, *Search for light scalar dark matter with atomic gravitational wave detectors*, *Phys. Rev. D* **97** (2018) 075020, [1606.04541].

[41] S. Abend, M. Gersemann, C. Schubert, D. Schlippert, E. M. Rasel, M. Zimmermann et al., *Atom interferometry and its applications*, 2001.10976.

[42] S. Dimopoulos, P. W. Graham, J. M. Hogan, M. A. Kasevich and S. Rajendran, *Atomic gravitational wave interferometric sensor*, *Phys. Rev. D* **78** (Dec, 2008) 122002.

[43] P. W. Graham, J. M. Hogan, M. A. Kasevich and S. Rajendran, *New method for gravitational wave detection with atomic sensors*, *Phys. Rev. Lett.* **110** (Apr, 2013) 171102.

[44] T. Mazzoni, X. Zhang, R. Del Aguila, L. Salvi, N. Poli and G. M. Tino, *Large-momentum-transfer Bragg interferometer with strontium atoms*, *Phys. Rev. A* **92** (2015) 053619, [1510.07939].

[45] J. Rudolph, T. Wilkason, M. Nantel, H. Swan, C. M. Holland, Y. Jiang et al., *Large Momentum Transfer Clock Atom Interferometry on the 689 nm Intercombination Line of Strontium*, *Phys. Rev. Lett.* **124** (2020) 083604, [1910.05459].

[46] J. N. Kirsten-Siemß, F. Fitzek, C. Schubert, E. M. Rasel, N. Gaaloul and K. Hammerer, *Large-Momentum-Transfer Atom Interferometers with μrad-Accuracy Using Bragg Diffraction*, *Phys. Rev. Lett.* **131** (2023) 033602, [2208.06647].

[47] J. M. McGuirk, M. J. Snadden and M. A. Kasevich, *Large area light-pulse atom interferometry*, *Phys. Rev. Lett.* **85** (Nov, 2000) 4498–4501.

[48] P. L. Bender, *Comparison of atom interferometry with laser interferometry for gravitational wave observations in space*, *Phys. Rev. D* **89** (Mar, 2014) 062004.

[49] S. Loriani et al., *Atomic source selection in space-borne gravitational wave detection*, *New J. Phys.* **21** (2019) 063030, [1812.11348].

[50] MAGIS collaboration, P. W. Graham, J. M. Hogan, M. A. Kasevich, S. Rajendran and R. W. Romani,

Mid-band gravitational wave detection with precision atomic sensors, 1711.02225.

[51] L. Badurina, O. Buchmueller, J. Ellis, M. Lewicki, C. McCabe and V. Vaskonen, *Prospective sensitivities of atom interferometers to gravitational waves and ultralight dark matter*, *Phil. Trans. A. Math. Phys. Eng. Sci.* **380** (2021) 20210060, [2108.02468].

[52] S. Abend et al., *Terrestrial Very-Long-Baseline Atom Interferometry: Workshop Summary*, 2310.08183.

[53] L. Badurina et al., *AION: An Atom Interferometer Observatory and Network*, *JCAP* **05** (2020) 011, [1911.11755].

[54] M. Abe, P. Adamson, M. Borcean, D. Bortoletto, K. Bridges, S. P. Carman et al., *Matter-wave atomic gradiometer interferometric sensor (magis-100)*, *Quantum Science and Technology* **6** (July, 2021) 044003.

[55] J. Hartwig, S. Abend, C. Schubert, D. Schlippert, H. Ahlers, K. Posso-Trujillo et al., *Testing the universality of free fall with rubidium and ytterbium in a very large baseline atom interferometer*, *New Journal of Physics* **17** (mar, 2015) 035011.

[56] L. von der Wense et al., *Direct detection of the 229Th nuclear clock transition*, *Nature* **533** (2016) 47–51, [1710.11398].

[57] P. G. Thirolf, S. Kraemer, D. Moritz and K. Scharl, *The thorium isomer* ^{229m}Th*: review of status and perspectives after more than 50 years of research*, *Eur. Phys. J. Spec. Top.* (2024) .

[58] E. Peik and C. Tamm, *Nuclear laser spectroscopy of the 3.5 ev transition in th-229*, *Europhysics Letters* **61** (jan, 2003) 181.

[59] C. J. Campbell, A. G. Radnaev, A. Kuzmich, V. A. Dzuba, V. V. Flambaum and A. Derevianko, *Single-ion nuclear clock for metrology at the 19th decimal place*, *Phys. Rev. Lett.* **108** (Mar, 2012) 120802.

[60] W. G. Rellergert, D. DeMille, R. R. Greco, M. P. Hehlen, J. R. Torgerson and E. R. Hudson, *Constraining the evolution of the fundamental constants with a solid-state optical frequency reference based on the* ^{229}Th *nucleus*, *Phys. Rev. Lett.* **104** (May, 2010) 200802.

[61] V. V. Flambaum, *Enhanced effect of temporal variation of the fine structure constant and the strong interaction in* ^{229}Th, *Phys. Rev. Lett.* **97** (Aug, 2006) 092502.

[62] V. V. Flambaum, N. Auerbach and V. F. Dmitriev, *Coulomb energy contribution to the excitation energy in Th-229*, *EPL* **85** (2009) 50005, [0807.3218].

[63] J. C. Berengut, V. A. Dzuba, V. V. Flambaum and S. G. Porsev, *Proposed experimental method to determine α sensitivity of splitting between ground and 7.6 ev isomeric states in* ^{229}Th, *Phys. Rev. Lett.* **102** (May, 2009) 210801.

[64] B. Seiferle et al., *Energy of the* ^{229}Th *nuclear clock transition*, *Nature* **573** (2019) 243–246, [1905.06308].

[65] B. R. Beck, J. A. Becker, P. Beiersdorfer, G. V. Brown, K. J. Moody, J. B. Wilhelmy et al., *Energy Splitting of the Ground-State Doublet in the Nucleus Th-229*, *Phys. Rev. Lett.* **98** (2007) 142501.

[66] J. C. Berengut and V. V. Flambaum, *Astronomical and laboratory searches for space-time variation of fundamental constants*, *Journal of Physics: Conference Series* **264** (Jan., 2011) 012010.

[67] P. Fadeev, J. C. Berengut and V. V. Flambaum,

[68] A. Caputo, D. Gazit, H.-W. Hammer, J. Kopp, G. Paz, G. Perez et al., *On the sensitivity of nuclear clocks to new physics*, 2407.17526.

[69] M. G. Kozlov, M. S. Safronova, J. R. Crespo López-Urrutia and P. O. Schmidt, *Highly charged ions: Optical clocks and applications in fundamental physics*, *Rev. Mod. Phys.* **90** (2018) 045005, [1803.06532].

[70] E. Peik, T. Schumm, M. S. Safronova, A. Pálffy, J. Weitenberg and P. G. Thirolf, *Nuclear clocks for testing fundamental physics*, *Quantum Sci. Technol.* **6** (2021) 034002, [2012.09304].

[71] P. G. Thirolf, B. Seiferle and L. von der Wense, *Fundamental Constants: Improving Our Knowledge on the 229mThorium Isomer: Toward a Test Bench for Time Variations of Fundamental Constants (Ann. Phys. 5/2019)*, *Annalen Phys.* **531** (2019) 1970022.

[72] A. Derevianko and M. Pospelov, *Hunting for topological dark matter with atomic clocks*, *Nature Phys.* **10** (2014) 933, [1311.1244].

[73] A. Banerjee, H. Kim, O. Matsedonskyi, G. Perez and M. S. Safronova, *Probing the Relaxed Relaxion at the Luminosity and Precision Frontiers*, *JHEP* **07** (2020) 153, [2004.02899].

[74] E. Fuchs, F. Kirk, E. Madge, C. Paranjape, E. Peik, G. Perez et al., *Implications of the laser excitation of the Th-229 nucleus for dark matter searches*, 2407.15924.

[75] B. Seiferle, L. von der Wense and P. G. Thirolf, *Lifetime Measurement of the Th229 nuclear isomer*, *Phys. Rev. Lett.* **118** (2017) 042501, [1801.05205].

[76] G. A. Kazakov, A. N. Litvinov, V. I. Romanenko, L. P. Yatsenko, A. V. Romanenko, M. Schreitl et al., *Performance of a 229thorium solid-state nuclear clock*, *New Journal of Physics* **14** (aug, 2012) 083019.

[77] S. Kraemer et al., *Observation of the radiative decay of the* ^{229}Th *nuclear clock isomer*, *Nature* **617** (2023) 706–710, [2209.10276].

[78] J. Thielking, K. Zhang, J. Tiedau, J. Zander, G. Zitzer, M. Okhapkin et al., *Vacuum-ultraviolet laser source for spectroscopy of trapped thorium ions*, *New journal of physics* **25** (Aug., 2023) 083026.

[79] J. Tiedau et al., *Laser Excitation of the Th-229 Nucleus*, *Phys. Rev. Lett.* **132** (2024) 182501.

[80] K. Beeks et al., *Growth and characterization of thorium-doped calcium fluoride single crystals*, *Sci. Rep.* **13** (2023) 3897, [2211.05445].

[81] R. Elwell, C. Schneider, J. Jeet, J. E. S. Terhune, H. W. T. Morgan, A. N. Alexandrova et al., *Laser Excitation of the Th229 Nuclear Isomeric Transition in a Solid-State Host*, *Phys. Rev. Lett.* **133** (2024) 013201, [2404.12311].

[82] C. Zhang et al., *Dawn of a nuclear clock: frequency ratio of the* ^{229m}Th *isomeric transition and the* ^{87}Sr *atomic clock*, 2406.18719.

[83] M. Jiang, B. D. Pecjak, G. Perez and S. Sankaranarayanan, *Lorentz violating backgrounds from quadratic, shift-symmetric, ultralight dark matter*, 2404.17636.

[84] D. Cyncynates and O. Simon, *Minimal targets for dilaton direct detection*, 2408.16816.

[85] T. Damour and J. F. Donoghue, *Equivalence Principle*

Violations and Couplings of a Light Dilaton, *Phys. Rev. D* **82** (2010) 084033, [`1007.2792`].

[86] M. Pospelov, *CP odd interaction of axion with matter*, *Phys. Rev. D* **58** (1998) 097703, [`hep-ph/9707431`].

[87] M. Pospelov, *Best values for the CP odd meson nucleon couplings from supersymmetry*, *Phys. Lett. B* **530** (2002) 123–128, [`hep-ph/0109044`].

[88] M. Pospelov and A. Ritz, *Electric dipole moments as probes of new physics*, *Annals Phys.* **318** (2005) 119–169, [`hep-ph/0504231`].

[89] J. I. Read, *The Local Dark Matter Density*, *J. Phys. G* **41** (2014) 063101, [`1404.1938`].

[90] G. P. Centers et al., *Stochastic fluctuations of bosonic dark matter*, *Nature Commun.* **12** (2021) 7321, [`1905.13650`].

[91] N. W. Evans, C. A. J. O'Hare and C. McCabe, *Refinement of the standard halo model for dark matter searches in light of the Gaia Sausage*, *Phys. Rev. D* **99** (2019) 023012, [`1810.11468`].

[92] L. Badurina, D. Blas and C. McCabe, *Refined ultralight scalar dark matter searches with compact atom gradiometers*, *Phys. Rev. D* **105** (2022) 023006, [`2109.10965`].

[93] J. Le Gouët, T. Mehlstäubler, J. Kim, S. Merlet, A. Clairon, A. Landragin et al., *Limits to the sensitivity of a low noise compact atomic gravimeter*, *Applied Physics B* **92** (June, 2008) 133–144.

[94] W. M. Itano, J. C. Bergquist, J. J. Bollinger, J. M. Gilligan, D. J. Heinzen, F. L. Moore et al., *Quantum projection noise: Population fluctuations in two-level systems*, *Phys. Rev. A* **47** (May, 1993) 3554–3570.

[95] A. Sugarbaker, M. Kasevich, P. Graham, G. Gratta and S. U. D. of Physics, *Atom Interferometry in a 10 M Fountain*. Stanford University, 2014.

[96] G. Santarelli, P. Laurent, P. Lemonde, A. Clairon, A. G. Mann, S. Chang et al., *Quantum projection noise in an atomic fountain: A high stability cesium frequency standard*, *Phys. Rev. Lett.* **82** (Jun, 1999) 4619–4622.

[97] S. Bize, P. Laurent, M. Abgrall, H. Marion, I. Maksimovic, L. Cacciapuoti et al., *Cold atom clocks and applications*, *Journal of Physics B: Atomic, Molecular and Optical Physics* **38** (2005) S449–S468.

[98] H. Muller, S.-w. Chiow, S. Herrmann, S. Chu and K.-Y. Chung, *Atom Interferometry tests of the isotropy of post-Newtonian gravity*, *Phys. Rev. Lett.* **100** (2008) 031101, [`0710.3768`].

[99] S. Dimopoulos, P. W. Graham, J. M. Hogan, M. A. Kasevich and S. Rajendran, *An Atomic Gravitational Wave Interferometric Sensor (AGIS)*, *Phys. Rev. D* **78** (2008) 122002, [`0806.2125`].

[100] S. Dimopoulos, P. W. Graham, J. M. Hogan and M. A. Kasevich, *General Relativistic Effects in Atom Interferometry*, *Phys. Rev. D* **78** (2008) 042003, [`0802.4098`].

[101] J. T. Mitchell, T. Kovachy, S. Hahn, P. Adamson and S. Chattopadhyay, *MAGIS-100 environmental characterization and noise analysis*, *JINST* **17** (2022) P01007, [`2202.04763`].

[102] E. V. Tkalya, C. Schneider, J. Jeet and E. R. Hudson, *Radiative lifetime and energy of the low-energy isomeric level in* ^{229}*Th*, *Phys. Rev. C* **92** (2015) 054324, [`1509.09101`].

[103] L. P. Parazzoli, A. M. Hankin and G. W. Biedermann,

Observation of free-space single-atom matter wave interference, *Physical Review Letters* **109** (Dec., 2012) .

[104] P. W. Graham, J. M. Hogan, M. A. Kasevich and S. Rajendran, *Resonant mode for gravitational wave detectors based on atom interferometry*, *Phys. Rev. D* **94** (2016) 104022, [`1606.01860`].

[105] G. M. Tino et al., *SAGE: A Proposal for a Space Atomic Gravity Explorer*, *Eur. Phys. J. D* **73** (2019) 228, [`1907.03867`].

[106] AEDGE collaboration, Y. A. El-Neaj et al., *AEDGE: Atomic Experiment for Dark Matter and Gravity Exploration in Space*, *EPJ Quant. Technol.* **7** (2020) 6, [`1908.00802`].

[107] J. M. Hogan, D. M. S. Johnson and M. A. Kasevich, *Light-pulse atom interferometry*, 2008.

[108] J.-M. Cui, S.-J. Sun, X.-W. Luo, Y.-F. Huang, C.-F. Li and G.-C. Guo, *Cold hybrid electrical-optical ion trap*, `2306.10366`.

[109] U. Schmidt, T. Bitter, P. El-Muzeini, D. Dubbers and O. Schärpf, *Long distance propagation of a polarized neutron beam in zero magnetic field*, *Nuclear Instruments and Methods in Physics Research Section A: Accelerators, Spectrometers, Detectors and Associated Equipment* **320** (1992) 569–573.

[110] E. Wodey et al., *A scalable high-performance magnetic shield for Very Long Baseline Atom Interferometry*, *Rev. Sci. Instrum.* **91** (2020) 035117, [`1911.12320`].

[111] I. Altarev et al., *A large-scale magnetic shield with 10^6 damping at mHz frequencies*, *J. Appl. Phys.* **117** (2015) 183903, [`1501.07861`].

[112] S. Dickerson, J. M. Hogan, D. M. S. Johnson, T. Kovachy, A. Sugarbaker, S.-w. Chiow et al., *A high-performance magnetic shield with large length-to-diameter ratio*, *Review of Scientific Instruments* **83** (06, 2012) 065108.

[113] C. Constable, *Earth's Electromagnetic Environment*, *Surveys in Geophysics* **37** (Jan., 2016) 27–45.

[114] C. Constable and S. Constable, *A grand spectrum of the geomagnetic field*, *Physics of the Earth and Planetary Interiors* **344** (2023) 107090.

[115] J. W. Sari and N. F. Ness, *Power Spectra of the Interplanetary Magnetic Field*, *Solar Physics* **8** (July, 1969) 155–165.

[116] S. Vitale, L. Sala, V. Ferroni and W. J. Weber, *Estimate of force noise from electrostatic patch potentials in lisa pathfinder*, 2024.

[117] D. Steck, "Quantum and atom optics." `http://steck.us/teaching`, 2007.

[118] M. O. Scully and M. S. Zubairy, *Quantum Optics*. Cambridge University Press, 1997.

[119] D. Schlippert, *Quantum tests of the universality of free fall*, phd thesis, Leibniz Universität Hannover, 2014.

[120] H. Metcalf and P. Van der Straten, *Laser Cooling and Trapping*. Graduate texts in contemporary physics. Springer, 1999.

[121] L. Salvi, N. Poli, V. Vuletić and G. M. Tino, *Squeezing on momentum states for atom interferometry*, *Phys. Rev. Lett.* **120** (Jan, 2018) 033601.

[122] P. V. Borisyuk, N. N. Kolachevsky, A. V. Taichenachev, E. V. Tkalya, I. Y. Tolstikhina and V. I. Yudin, *Excitation of the low-energy* ^{229m}*Th isomer in the electron bridge process via the continuum*, *Phys. Rev. C* **100** (Oct, 2019) 044306.

[123] M. F. Gu, *The flexible atomic code*, *Canadian Journal of Physics* **86** (2008) 675–689, [https://doi.org/10.1139/p07-197].

[124] L. von der Wense, P. V. Bilous, B. Seiferle, S. Stellmer, J. Weitenberg, P. G. Thirolf et al., *The theory of direct laser excitation of nuclear transitions*, *Eur. Phys. J. A* **56** (2020) 176, [2001.08320].

[125] M. S. Lubell and W. Raith, *Polarization effect in photoionization of cesium*, *Phys. Rev. Lett.* **23** (Aug, 1969) 211–214.

[126] R. A. Fox, R. M. Kogan and E. J. Robinson, *Laser triple-quantum photoionization of cesium*, *Phys. Rev. Lett.* **26** (Jun, 1971) 1416–1417.

[127] C.-H. Li and D. Budker, *Polarization-dependent photoionization cross sections and radiative lifetimes of atomic states in* Ba I, *Phys. Rev. A* **74** (Jul, 2006) 012512.

[128] F. Thini, K. L. Romans, B. P. Acharya, A. H. N. C. de Silva, K. Compton, K. Foster et al., *Photo-ionization of polarized lithium atoms out of an all-optical atom trap: a complete experiment*, *Journal of Physics B: Atomic, Molecular and Optical Physics* **53** (Mar., 2020) 095201.

[129] A. M. Popov, O. V. Tikhonova and E. A. Volkova, *Strong-field atomic stabilization: numerical simulation and analytical modelling*, *Journal of Physics B: Atomic, Molecular and Optical Physics* **36** (apr, 2003) R125.

[130] M. V. Fedorov, *Stabilization of Atoms in a Strong Laser Field*, pp. 1–18. Springer Berlin Heidelberg, Berlin, Heidelberg, 2006. 10.1007/3-540-34422-5_1.

[131] M. Pont and M. Gavrila, *Stabilization of atomic hydrogen in superintense, high-frequency laser fields of circular polarization*, *Phys. Rev. Lett.* **65** (Nov, 1990) 2362–2365.

[132] M. V. Fedorov and N. P. Poluektov, *Two-color interference stabilization of atoms*, *Phys. Rev. A* **69** (Mar, 2004) 033404.

[133] J. W. Cooper, *Photoionization from outer atomic subshells. a model study*, *Phys. Rev.* **128** (Oct, 1962) 681–693.

[134] U. FANO and J. W. COOPER, *Spectral distribution of atomic oscillator strengths*, *Rev. Mod. Phys.* **40** (Jul, 1968) 441–507.

[135] I. Gilary, Y. Sajeev, M. F. Ciappina, A. Croy, C. M. Goletz, S. Klaiman et al., *Suppression of photoionization by a static field*, *Phys. Rev. Lett.* **101** (Oct, 2008) 163002.

[136] J. Harms, *Terrestrial Gravity Fluctuations*, *Living Rev. Rel.* **18** (2015) 3, [1507.05850].

[137] S. A. Hughes and K. S. Thorne, *Seismic gravity-gradient noise in interferometric gravitational-wave detectors*, *Phys. Rev. D* **58** (Nov, 1998) 122002.

[138] F. Vetrano and A. Viceré, *Newtonian noise limit in atom interferometers for gravitational wave detection*, *Eur. Phys. J. C* **73** (2013) 2590, [1304.1702].

[139] J. G. Baker and J. I. Thorpe, *Comparison of atom interferometers and light interferometers as space-based gravitational wave detectors*, *Phys. Rev. Lett.* **108** (May, 2012) 211101.

[140] J. Harms, B. J. J. Slagmolen, R. X. Adhikari, M. C. Miller, M. Evans, Y. Chen et al., *Low-frequency terrestrial gravitational-wave detectors*, *Phys. Rev. D*

[141] L. Badurina, V. Gibson, C. McCabe and J. Mitchell, *Ultralight dark matter searches at the sub-Hz frontier with atom multigradiometry*, *Phys. Rev. D* **107** (2023) 055002, [2211.01854].

[142] J. Peterson, *Observations and Modeling of Seismic Background Noise.* DIANE Publishing Company, 2003.

[143] G. L. Smith, C. D. Hoyle, J. H. Gundlach, E. G. Adelberger, B. R. Heckel and H. E. Swanson, *Short-range tests of the equivalence principle*, *Phys. Rev. D* **61** (Dec, 1999) 022001.

[144] S. Schlamminger, K. Y. Choi, T. A. Wagner, J. H. Gundlach and E. G. Adelberger, *Test of the equivalence principle using a rotating torsion balance*, *Phys. Rev. Lett.* **100** (2008) 041101, [0712.0607].

[145] P. Touboul et al., *MICROSCOPE Mission: First Results of a Space Test of the Equivalence Principle*, *Phys. Rev. Lett.* **119** (2017) 231101, [1712.01176].

[146] J. Bergé, P. Brax, G. Métris, M. Pernot-Borràs, P. Touboul and J.-P. Uzan, *MICROSCOPE Mission: First Constraints on the Violation of the Weak Equivalence Principle by a Light Scalar Dilaton*, *Phys. Rev. Lett.* **120** (2018) 141101, [1712.00483].

[147] A. Hees, O. Minazzoli, E. Savalle, Y. V. Stadnik and P. Wolf, *Violation of the equivalence principle from light scalar dark matter*, *Phys. Rev. D* **98** (2018) 064051, [1807.04512].

[148] A. Hees, J. Guéna, M. Abgrall, S. Bize and P. Wolf, *Searching for an oscillating massive scalar field as a dark matter candidate using atomic hyperfine frequency comparisons*, *Phys. Rev. Lett.* **117** (2016) 061301, [1604.08514].

[149] A. Branca et al., *Search for an Ultralight Scalar Dark Matter Candidate with the AURIGA Detector*, *Phys. Rev. Lett.* **118** (2017) 021302, [1607.07327].

[150] C. J. Kennedy, E. Oelker, J. M. Robinson, T. Bothwell, D. Kedar, W. R. Milner et al., *Precision Metrology Meets Cosmology: Improved Constraints on Ultralight Dark Matter from Atom-Cavity Frequency Comparisons*, *Phys. Rev. Lett.* **125** (2020) 201302, [2008.08773].

[151] T. Kobayashi, A. Takamizawa, D. Akamatsu, A. Kawasaki, A. Nishiyama, K. Hosaka et al., *Search for ultralight dark matter from long-term frequency comparisons of optical and microwave atomic clocks*, *Physical Review Letters* **129** (Dec., 2022) .

[152] N. Sherrill et al., *Analysis of atomic-clock data to constrain variations of fundamental constants*, *New J. Phys.* **25** (2023) 093012, [2302.04565].

[153] A. Banerjee, D. Budker, M. Filzinger, N. Huntemann, G. Paz, G. Perez et al., *Oscillating nuclear charge radii as sensors for ultralight dark matter*, 2301.10784.

[154] I. Kozyryev, Z. Lasner and J. M. Doyle, *Enhanced sensitivity to ultralight bosonic dark matter in the spectra of the linear radical sroh*, *Physical Review A* **103** (Apr., 2021) .

[155] K. K. Rogers and H. V. Peiris, *Strong Bound on Canonical Ultralight Axion Dark Matter from the Lyman-Alpha Forest*, *Phys. Rev. Lett.* **126** (2021) 071302, [2007.12705].

[156] W. Zhao, H. Liu and X. Mei, *Ultralight scalar and axion dark matter detection with atom interferometers*, 2401.17055.

[157] H. Kim and G. Perez, *Oscillations of atomic energy*

levels induced by QCD axion dark matter, *Phys. Rev. D* **109** (2024) 015005, [2205.12988].

[158] T. Wilkason, M. Nantel, J. Rudolph, Y. Jiang, B. E. Garber, H. Swan et al., *Atom Interferometry with Floquet Atom Optics*, *Phys. Rev. Lett.* **129** (2022) 183202, [2205.06965].

[159] J. T. VanderPlas, *Understanding the lomb–scargle periodogram*, *The Astrophysical Journal Supplement Series* **236** (may, 2018) 16.

[160] D. Budker, P. W. Graham, M. Ledbetter, S. Rajendran and A. Sushkov, *Proposal for a Cosmic Axion Spin Precession Experiment (CASPEr)*, *Phys. Rev. X* **4** (2014) 021030, [1306.6089].

[161] H. C. Torrey, *Transient nutations in nuclear magnetic resonance*, *Phys. Rev.* **76** (Oct, 1949) 1059–1068.

[162] H.-R. Noh and W. Jhe, *Analytic solutions of the optical bloch equations*, *Optics Communications* **283** (2010) 2353–2355.

[163] H. Hachisu, G. Petit, F. Nakagawa, Y. Hanado and T. Ido, *Si-traceable measurement of an optical frequency at the low $10-16$ level without a local primary standard*, *Opt. Express* **25** (Apr, 2017) 8511–8523.

[164] E. J. Angstmann, V. A. Dzuba and V. V. Flambaum, *Relativistic effects in two valence-electron atoms and ions and the search for variation of the fine-structure constant*, *Physical Review A* **70** (July, 2004) .